

# Photon motion in Kerr–de Sitter spacetimes

Daniel Charbulák\* and Zdeněk Stuchlík†

*Institute of Physics and Research Centre of Theoretical Physics and Astrophysics,  
Faculty of Philosophy and Science, Silesian university in Opava,  
Bezručovo nám. 13, CZ-746 01 Opava, Czech Republic*

(Dated: March 6, 2017)

We study general non-equatorial motion of photons in the Kerr-de Sitter black hole and naked singularity spacetimes. The motion is governed by the impact parameter  $X$  related to axial symmetry of the spacetime, and impact parameter  $q$  related to its hidden symmetry. Appropriate 'effective potentials' governing the latitudinal and radial motion are introduced and their behaviour is examined by 'Chinese boxes' technique giving regions allowed for the motion in terms of the impact parameters. Limits on the impact parameter  $X$  and  $q$  are established in dependence on the spacetime parameters  $M, \Lambda, a$ . The motion can be of orbital type (crossing the equatorial plane,  $q > 0$ ) and vortical type (tied above or below the equatorial plane,  $q < 0$ ). It is shown that for negative values of  $q$  the reality conditions imposed on the latitudinal motion yield stronger constraints on the parameter  $X$  than that following from the reality condition of motion in the radial direction, which, e. g., exclude possibility of existence of vortical motion of constant radius. Several other consequences are determined and a classification of Kerr–de Sitter spacetimes reflecting the behaviour of the effective potentials is given.

## I. INTRODUCTION

In the framework of inflationary paradigm [38], recent cosmological observations indicate that a very small relict vacuum energy (equivalently, repulsive cosmological constant  $\Lambda > 0$ ), or, generally, a dark energy demonstrating repulsive gravitational effect, has to be introduced to explain dynamics of the recent Universe [3, 6, 13, 34, 35, 42, 83]. These conclusions are supported strongly by the observations of distant Ia-type supernova explosions indicating that starting at the cosmological redshift  $z \approx 1$  expansion of the Universe is accelerated [48]. The total energy density of the Universe is very close to the critical energy density  $\rho_{\text{crit}}$  corresponding to almost flat universe predicted by the inflationary scenario [55], and the dark energy represents about 70% of the energy content of the observable universe [12, 56]. These conclusions are confirmed by recent measurements of cosmic microwave background anisotropies by the space satellite observatory PLANCK [1, 45].

The dark energy equation of state is very close to those corresponding to the vacuum energy [12]. Therefore, it is relevant to study the astrophysical consequences of the effect of the observed cosmological constant implied by the cosmological tests to be  $\Lambda \approx 1.3 \times 10^{-56} \text{ cm}^{-2}$ , and the related vacuum energy  $\rho_{\text{vac}} \sim 10^{-29} \text{ g/cm}^3$ , close to the critical density of the universe. The repulsive cosmological constant changes significantly the asymptotic structure of black-hole, naked singularity, or any compact-body backgrounds as such backgrounds become asymptotically de Sitter spacetimes, and an event horizon (cosmological horizon) always exists, behind which

the geometry is dynamic.

Substantial influence of the repulsive cosmological constant has been demonstrated for astrophysical situations related to active galactic nuclei and their central supermassive black holes [62]. The black hole spacetimes with the  $\Lambda$  term are described in the spherically symmetric case by the vacuum Schwarzschild–de Sitter (SdS) geometry [30, 65], while the internal, uniform density SdS spacetimes are given in [10, 61]. The axially symmetric, rotating black holes are determined by the Kerr–de Sitter (KdS) geometry [14, 21]. In the spacetimes with the repulsive cosmological term, motion of photons was extensively investigated in many papers [7, 37, 40, 50, 51, 64, 66, 82]. The motion of massive test particles was studied in [2, 15, 16, 25, 27, 28, 31–33, 41, 44, 52, 59, 60, 65, 67, 78]. The KdS geometry can be relevant also for the so called Kerr superspinars representing an alternative to black holes [11, 22, 23, 76], breaking the black hole bound on the dimensionless spin and exhibiting a variety of unusual physical phenomena [17, 18, 26, 57, 69, 73, 76, 77]. It is worth to note that the SdS and KdS spacetimes are equivalent to some solutions of the  $f(R)$  gravity representing black holes and naked singularities [43, 80].

The role of the cosmological constant can be significant for both the geometrically thin Keplerian accretion discs [39, 54, 62, 65, 78] and the toroidal accretion discs [5, 36, 46, 47, 53, 79, 81] orbiting supermassive black holes (Kerr superspinars) in the central parts of giant galaxies. Both high-frequency quasiperiodic oscillations and jets originating at the accretion discs can be reflected by current carrying string loops in SdS and KdS spacetimes [24, 29, 70, 71, 84]. In the spherically symmetric spacetimes, the Keplerian and toroidal disc structures can be precisely described the Pseudo-Newtonian potential of Paczynski type [72, 80] that appears to be useful also in studies of motion of interacting

\*Electronic address: daniel.charbulak@fpf.slu.cz

†Electronic address: zdenek.stuchlik@fpf.slu.cz

galaxies [49, 74, 75] demonstrating relation of the gravitationally bound galactic systems to the so called static radius of the SdS or KdS spacetimes [4, 19, 20, 59, 60]. This idea has been confirmed by the recent study of general relativistic static polytropic spheres in spacetimes with the repulsive cosmological constant [68].

The present paper is devoted to detailed study of properties of the photon motion in the KdS black hole and naked singularity spacetimes. We concentrate attention to the behavior of the effective potentials determining the regions allowed for the photon motion. Such a study is necessary for full understanding of the optical phenomena occurring in the black hole or naked singularity spacetimes with the repulsive cosmological constant. We generalize the previous work concentrated on the properties of the photon motion in the equatorial plane [66], discussing properties of the effective potential of the latitudinal motion in terms of the motion constant related to the equatorial plane, and then continuing by study of the effective potential of the radial motion.

## II. KERR-DE SITTER SPACETIME AND CARTER'S EQUATIONS OF GEODESIC MOTION

### A. Kerr-de Sitter geometry

The line element describing the Kerr-de Sitter geometry is in the standard Boyer-Lindquist coordinates, using geometric system of units ( $c = G = 1$ ), given by

$$ds^2 = - \frac{\Delta_r}{I^2 \rho^2} (dt - a \sin^2 \theta d\phi)^2 + \frac{\Delta_\theta \sin^2 \theta}{I^2 \rho^2} [a dt - (r^2 + a^2) d\phi]^2 + \frac{\rho^2}{\Delta_r} dr^2 + \frac{\rho^2}{\Delta_\theta} d\theta^2, \quad (1)$$

where

$$\Delta_r = \left(1 - \frac{1}{3}\Lambda r^2\right) (r^2 + a^2) - 2Mr, \quad (2)$$

$$\Delta_\theta = 1 + \frac{1}{3}\Lambda a^2 \cos^2 \theta, \quad (3)$$

$$I = 1 + \frac{1}{3}\Lambda a^2, \quad (4)$$

$$\rho^2 = r^2 + a^2 \cos^2 \theta. \quad (5)$$

Here, as usual, we denoted by  $M$  the mass of the central gravitating body, by  $a$  its specific angular momentum ( $a = J/M$ ) and by  $\Lambda$  the cosmological constant. In order to simplify the discussion of the following equations, it is convenient to introduce a new cosmological parameter  $y = \frac{1}{3}\Lambda M^2$ , and use dimensionless quantities, redefining them such that  $s/M \rightarrow s$ ,  $t/M \rightarrow t$ ,  $r/M \rightarrow r$ ,  $a/M \rightarrow a$ , which is equivalent to putting  $M = 1$ . The above expres-

sions then read

$$\Delta_r = (1 - yr^2) (r^2 + a^2) - 2r, \quad (6)$$

$$\Delta_\theta = 1 + a^2 y \cos^2 \theta, \quad (7)$$

$$I = 1 + a^2 y, \quad (8)$$

with equation (5) being left unchanged.

The physical singularity is located, as in the Kerr geometry, at the ring  $r = 0$ ,  $\theta = \pi/2$ .

The black hole horizons are determined by the condition

$$\Delta_r = 0 \quad (9)$$

and their loci can be determined by the relation

$$y = y_h(r; a^2) \equiv \frac{r^2 - 2r + a^2}{r^2(r^2 + a^2)}. \quad (10)$$

The zeros of  $y_h(r; a^2)$ , determining the loci of black hole horizons in pure Kerr spacetimes, are given by the relation

$$a^2 = a_{z(h)}^2(r) \equiv 2r - r^2, \quad (11)$$

the loci of its extrema are given by the functions

$$a^2 = a_{ex(h)\pm}^2(r) \equiv \frac{r(1 - 2r \pm \sqrt{1 + 8r})}{2}, \quad (12)$$

where the function  $a_{ex(h)-}^2(r) < 0$  in its whole definition range, hence is irrelevant. The functions  $y_h(r; a^2)$ ,  $a_{z(h)}^2(r)$  and  $a_{ex(h)\pm}^2(r)$  will be needed in the section devoted to the discussion of the radial motion.

Three event horizons, two black hole  $r_-$ ,  $r_+$ , and the cosmological horizon  $r_c$ , ( $r_- < r_+ < r_c$ ) exist for  $y_{min(h)}(a^2) < y < y_{max(h)}(a^2)$ , where the limits  $y_{min/max(h)}(a^2)$  correspond to local minimum or local maximum of the function  $y_h(r; a^2)$ , respectively, for given rotational parameter  $a$ . For  $0 < y < y_{min(h)}(a^2)$  or  $y > y_{max(h)}(a^2)$  Kerr-de Sitter naked singularity spacetimes exist. The limit case  $y = y_{min(h)}(a^2)$  corresponds to an extreme black hole spacetime, when the two black hole horizons coalesce. If  $y = y_{max(h)}(a^2)$ , the outer black hole and cosmological horizon merge. There exists critical value of the rotational parameter  $a_{crit}^2 = 1.21202$ , for which the two local extrema of the function  $y_h(r; a^2)$  coalesce in an inflection point at  $r_{crit} = 1.61603$  with the critical value  $y_{crit} = 0.0592$ . Thus, for  $a^2 > a_{crit}^2$  only Kerr-de Sitter naked singularity can exist for any  $y > 0$ .

Properties of the event horizons for the more general case of the Kerr-Newman-de Sitter spacetimes can be found in [66].

### B. Carter's equations of geodesic motion

The motion of test particles and photons following its geodesics in the Kerr-de Sitter spacetime is described by

the well known Carter equations [14]

$$\rho^2 \frac{d\theta}{d\lambda} = \pm \sqrt{W(\theta; E, \Phi, \mathcal{K}, y, a)}, \quad (13)$$

$$\rho^2 \frac{dr}{d\lambda} = \pm \sqrt{R(r; E, \Phi, \mathcal{K}, y, a)}, \quad (14)$$

$$\rho^2 \frac{d\varphi}{d\lambda} = \frac{aI^2[E(r^2 + a^2) - a\Phi]}{\Delta_r} - \frac{I^2[aE \sin^2 \theta - \Phi]}{\Delta_\theta \sin^2 \theta}, \quad (15)$$

$$\rho^2 \frac{dt}{d\lambda} = \frac{I^2(r^2 + a^2)[E(r^2 + a^2) - a\Phi]}{\Delta_r} - \frac{aI^2[aE \sin^2 \theta - \Phi]}{\Delta_\theta}, \quad (16)$$

where

$$W(\theta; E, \Phi, \mathcal{K}, y, a) = \mathcal{K}\Delta_\theta - \frac{I^2(aE \sin^2 \theta - \Phi)^2}{\sin^2 \theta} \quad (17)$$

and

$$R(r; E, \Phi, \mathcal{K}, y, a) = [IE(r^2 + a^2) - Ia\Phi]^2 - \Delta_r \mathcal{K}. \quad (18)$$

Here  $E$  and  $\Phi$  are the constants of motion connected respectively with the time and axial symmetry of the Kerr–de Sitter geometry, and  $\mathcal{K}$  is the fourth Carter constant of motion connected with the hidden symmetry of the Kerr–de Sitter geometry. Another constant of motion is the rest mass  $m$  (energy) of the test particle; for photons  $m = 0$ . Recall that  $E$  and  $\Phi$  cannot be interpreted as energy and axial component of the angular momentum of the test particle at infinity, because, due to the presence of the cosmological  $\Lambda$  term, the geometry is not asymptotically flat, but de Sitter [65].

Detailed discussion of the equatorial motion of photons in the Kerr–Newman–de Sitter spacetimes has been published in [66]. Circular motion of test particles in the Kerr–de Sitter spacetimes has been presented in [78]. Here we restrict our attention on the general motion of photons in the Kerr–de Sitter spacetimes.

In fact, the motion of photons is independent of the constant of motion  $E$  and depends only on the ratio  $\Phi/E$  ( $E \neq 0$ ), usually referred to as the impact parameter  $\ell$ , and on the parameter  $\mathcal{K}/E^2$ . For our general discussion it is convenient to use  $Q = \mathcal{K} - I^2(\Phi - aE)^2$  that vanishes for the equatorial motion. For our purposes it is, however, following the paper [66], convenient to introduce a new constants of motion  $X \equiv \ell - a$ . Further the constant  $q \equiv Q/I^2E^2$  will be applied. Then the relations (17) and (18) simplify to the form

$$W(\theta; X, q, y, a) \equiv I^2E^2[(X^2 + q)\Delta_\theta - \frac{(a \cos^2 \theta + X)^2}{\sin^2 \theta}], \quad (19)$$

$$R(r; X, q, y, a) \equiv I^2E^2[(r^2 - aX)^2 - \Delta_r(X^2 + q)]. \quad (20)$$

Following the work [66] we study the general photon motion in terms of the parameter  $X$ . However, since we consider the non-equatorial motion here, it is also necessary to find out the restrictions to be imposed on parameter  $X$  that follows from the reality conditions of the latitudinal motion. The latitudinal motion in the Kerr–de Sitter spacetimes has been investigated yet [59]; however, the discussion has been related to the motion constant  $\mathcal{K}$ . Here we give the discussion of the effective potential of the latitudinal motion related to the motion constant  $Q$ , as it is convenient for the purposes of our study.

### III. LATITUDINAL MOTION

Because it is more convenient to work with algebraic functions instead of trigonometric ones, we introduce a new variable

$$m = \cos^2 \theta,$$

$$dm = 2\text{sign}(\theta - \pi/2)\sqrt{m(1-m)}d\theta.$$

This implies replacing the equation (13) by

$$\rho^2 \frac{dm}{d\lambda} = \pm 2\sqrt{M(m; X, q, y, a)}, \quad (21)$$

where

$$M(m; X, q, y, a) \equiv I^2E^2m[(1-m)(X^2+q)\Delta_m - (am+X)^2] \quad (22)$$

with notation

$$\Delta_m = 1 + a^2ym. \quad (23)$$

Note that  $dm/d\lambda = 0$  does not necessarily imply  $d\theta/d\lambda = 0$ , since it can mean just transit through the equatorial plane or polar axis. Therefore, in some cases, in order to avoid any doubts, we rather discuss the behaviour of the function (19).

The reality condition  $M(m; a, y, X, q) \geq 0$  can be expressed by the relations

$$X_-^\theta(m; q, y, a) \leq X \leq X_+^\theta(m; q, y, a) \quad (24)$$

in regions where  $\Delta_m - a^2y > 0$ , i. e., equivalently,

$$m > m_d,$$

where

$$m_d = 1 - 1/a^2y \quad (25)$$

is the solution of the equation

$$\Delta_m - a^2y = 0, \quad (26)$$

and by the relations

$$X \leq X_+^\theta(m; q, y, a), \quad X_-^\theta(m; q, y, a) \leq X, \quad (27)$$

in regions where  $\Delta_m - a^2 y < 0$ , i. e.,  $m < m_d$ , which requires  $y > 1/a^2$ . The functions  $X_{\pm}^{\theta}(m; q, y, a)$ , regarded as 'effective potentials' governing the latitudinal motion, are defined by

$$X_{\pm}^{\theta}(m; q, y, a) \equiv \frac{-am \pm \sqrt{m(1-m)\Delta_m[a^2m + q(\Delta_m - a^2y)]}}{m(\Delta_m - a^2y)}. \quad (28)$$

The functions  $X_{\pm}^{\theta}(m; q, y, a)$  thus determine the regions allowed for the latitudinal motion, conditions  $X = X_{\pm}^{\theta}(m; q, y, a)$  give the turning points. In order to understand the behaviour of the functions  $X_{\pm}^{\theta}(m; q, y, a)$ , it is necessary to find the reality regions, and loci of its local extrema and divergencies. Following [66], we shall perform this analysis using the well known procedure called 'Chinese boxes technique' and adopting labelling of the appropriate characteristic functions in similar way. The parameters are of various significance -  $q$  is a constant of motion, whereas  $a, y$  govern the geometry. The natural choice is therefore to give the properties of the potentials  $X_{\pm}^{\theta}(m; q, y, a)$  by family of functions  $q(m; y, a)$ , and properties of these functions by another families of functions of variable  $m$  with parameters lowered by one, with spacetime parameters excluded at last.

In the following analysis the relevant range of variable  $m$  is, of course,  $0 \leq m \leq 1$ , but somewhere, in order to better understand the behaviour of the characteristic functions, we formally permit  $m \in R$ .

First we shall determine the reality region of  $X_{\pm}(m)$ . It is given by

$$q \geq q_r^{\theta}(m; y, a^2) \quad \text{if} \quad \Delta_m - a^2 y > 0, \quad (29)$$

$$q \leq q_r^{\theta}(m; y, a^2) \quad \text{if} \quad \Delta_m - a^2 y < 0, \quad (30)$$

where

$$q_r^{\theta}(m; y, a^2) \equiv \frac{a^2 m}{a^2 y - \Delta_m}. \quad (31)$$

Of course, this function also determines the common points of the potentials  $X_{-}^{\theta}(m; q, y, a)$  and  $X_{+}^{\theta}(m; q, y, a)$ , which values are then

$$X_c^{\theta} = X_{(\pm)}^{\theta}(m; q = q_r^{\theta}, y, a) = X_{(\pm)}^{\theta}(m; y, a) \equiv \frac{a}{a^2 y - \Delta_m}. \quad (32)$$

Of particular importance, if defined, is the value  $X_{(\pm)}^{\theta}(1; y, a) = -a$  (see below).

The divergency points of the functions  $q_r^{\theta}(m; y, a^2)$ ,  $X_{(\pm)}^{\theta}(m; y, a)$  and  $X_{-}^{\theta}(m; q, y, a)$  are determined by

$$y = y_d^{\theta}(m; a^2) \equiv \frac{1}{a^2(1-m)}. \quad (33)$$

Both the functions  $X_{\pm}^{\theta}(m; q, y, a)$  can diverge, if well defined, for  $m = 0$ , another divergencies are given by the function  $y_d^{\theta}(m; a^2)$  for the potential  $X_{-}^{\theta}(m; q, y, a)$ , but there are no other divergencies for the potential

$X_{+}^{\theta}(m; q, y, a)$ , as can be seen, if we rewrite the definition (29) in an alternative form

$$X_{\pm}^{\theta}(m; q, y, a) = \frac{a^2 m^2 - q(1-m)\Delta_m}{-am \mp \sqrt{m(1-m)\Delta_m[a^2m + q(\Delta_m - a^2y)]}}. \quad (34)$$

The function  $y_d^{\theta}(m; a^2) \rightarrow \infty$  for  $m \rightarrow 1$  from the left. There are no local extrema of this function and for  $0 \leq m < 1$  it is increasing. For  $m = 0$  we get  $y_d^{\theta}(0; a^2) = 1/a^2$ .

The point  $m_d$  given by the definition (25) determines the loci where the functions  $q_r^{\theta}(m; y, a^2)$ ,  $X_{(\pm)}^{\theta}(m; y, a)$  and  $X_{-}^{\theta}(m; q, y, a)$  diverge; it occurs at relevant interval  $(0; 1)$  for  $y > 1/a^2$  and  $m_d \rightarrow 1$  for  $a^2 y \rightarrow \infty$ . In such case,  $q_r^{\theta}(m; y, a^2) \rightarrow +\infty$  ( $-\infty$ ) for  $m \rightarrow m_d$  from the left (right).

From the equality

$$\partial q_r^{\theta} / \partial m = \frac{a^2(a^2 y - 1)}{(\Delta_m - a^2 y)^2} \quad (35)$$

one can see that the function  $q_r^{\theta}(m; y, a^2)$  has no local extrema and is decreasing for  $y < 1/a^2$ , or piecewise increasing with the discontinuity point  $m_d$  for  $y > 1/a^2$ , i. e.,  $q_r^{\theta}(m; y, a^2) \rightarrow +\infty$  ( $-\infty$ ) for  $m \rightarrow m_d$  from the left (right). It always holds  $q_r^{\theta}(m = 0; y, a^2) = 0$  and  $q_r^{\theta}(m = 1; y, a^2) = -a^2$ .

In the special case  $y = 1/a^2$  we get

$$q_r^{\theta}(m; y = 1/a^2, a^2) = \text{const.} = -a^2 \quad \text{for} \quad m \neq 0$$

with

$$\lim_{m \rightarrow 0} q_r^{\theta}(m; y = 1/a^2, a^2) = -a^2.$$

Based on the conditions (29), (30) and the above characteristic functions, we can complete setting the definition range of the potentials  $X_{\pm}^{\theta}(m; q, a, y)$ , which we leave to the end of this section.

Now we shall determine the loci of local extrema of the effective potentials  $X_{\pm}^{\theta}(m; q, y, a)$ . They can be derived from the condition  $\partial X_{\pm}^{\theta} / \partial m = 0$ , which implies the equation

$$(a^2 m^2 + q)(\Delta_m - a^2 y)[a^2 m^2 I^2 + q(1 - a^2 y + 2a^2 m y)^2] = 0. \quad (36)$$

It can be verified that the function  $X_{+}^{\theta}(m; q, y, a)$  has local extrema given by the relation

$$q = q_{ex(+)}^{\theta}(m; a^2) \equiv -a^2 m^2. \quad (37)$$

A discussion of this function is trivial, so we only note that it is independent of the cosmological parameter  $y$  and renders the loci of extrema only for  $-a^2 \leq q \leq 0$ , while, as we shall see below, they can exist even for  $q < -a^2$ . The character of these extrema reveals inserting this expression into the second derivative, which yields

$$\partial^2 X_{+}^{\theta} / \partial m^2(m; q = q_{ex(+)}^{\theta}, y, a) = \frac{-a}{m(1-m)\Delta_m}, \quad (38)$$

clearly they must be maxima.

From the equation (36) we find that another extrema of the potentials  $X_{\pm}^{\theta}(m; q, y, a)$  are determined by the condition

$$q = q_{ex(\pm)}^{\theta}(m; y, a^2) \equiv \frac{-a^2 m^2 I^2}{[\Delta_m - a^2 y(1 - m)]^2}. \quad (39)$$

The divergencies of the functions  $q_{ex(\pm)}^{\theta}(m; y, a^2)$  are determined by the relation

$$y = y_{d(ex\pm)}^{\theta}(m; a) \equiv \frac{1}{a^2(1 - 2m)}. \quad (40)$$

The function  $y_{d(ex\pm)}^{\theta}(m; a^2)$  is positively valued at  $0 \leq m < 0.5$ , where  $y_{d(ex\pm)}^{\theta}(m; a^2) \rightarrow +\infty$  for  $m \rightarrow 0.5$  from the left. For  $m = 0$ , there is  $y_{d(ex\pm)}^{\theta}(0; a^2) = y_{d(r)}^{\theta}(0; a^2) = 1/a^2$ .

From the properties of the function  $y_{d(ex\pm)}^{\theta}(m; a^2)$  we deduce that the function  $q_{ex(\pm)}^{\theta}(m; y, a^2)$  can diverge only if  $y > 1/a^2$ , at

$$m = m_{d(ex)} \equiv 0.5(1 - 1/a^2 y) = 0.5 m_d$$

located such that  $0 \leq m_{d(ex)} < 0.5$ . Obviously

$$q_{ex(\pm)}^{\theta}(m; y, a^2) \rightarrow -\infty \quad \text{for } m \rightarrow m_{d(ex)}. \quad (41)$$

In the following we shall decide about the monotony and possible existence of local extrema of the function  $q_{ex(\pm)}^{\theta}$ . From

$$\partial q_{ex(\pm)}^{\theta} / \partial m = \frac{2m(a^2 y - 1)a^2 I^2}{[\Delta_m - a^2 y(1 - m)]^3} \quad (42)$$

it is clear that there are no local extrema of  $q_{ex(\pm)}^{\theta}(m; y, a^2)$  in the interval  $m \in (0; 1)$ . The derivative changes its sign at the divergent point  $m_{d(ex)}$ , which reflects the behaviour given by (41). For  $y < 1/a^2$ , there is

$$\partial q_{ex(\pm)}^{\theta} / \partial m < 0 \quad \text{for } m \in (0; 1),$$

that is,  $q_{ex(\pm)}^{\theta}(m; y, a^2)$  is decreasing.

In the limit case  $y = 1/a^2$ , we get

$$q_{ex(\pm)}^{\theta}(m; y = 1/a^2, a^2) = -a^2 = q_r^{\theta}(m; y = 1/a^2, a^2).$$

Comparing both the functions  $q_{ex+}^{\theta}(m; a^2)$  and  $q_{ex-}^{\theta}(m; y, a^2)$ , we find that

$$q_{ex(\pm)}^{\theta}(m; y, a^2) \leq q_{ex+}^{\theta}(m; a^2) \leq 0$$

and have common points at  $m = 0, 1$  with

$$q_{ex+}^{\theta}(0; a^2) = q_{ex(\pm)}^{\theta}(0; y, a^2) = 0$$

and

$$q_{ex+}^{\theta}(1; a^2) = q_{ex(\pm)}^{\theta}(1; y, a^2) = -a^2.$$

In the next step we shall characterize the extrema given by  $q_{ex(\pm)}^{\theta}(m; y, a^2)$ . First we find that

$$\frac{\partial X_{\pm}^{\theta}}{\partial m}(m; q = q_{ex(\pm)}^{\theta}, y, a) = \frac{a^3 y \{ \text{sign}[1 - a^2 y(1 - 2m)] \pm \text{sign}(1 - a^2 y) \}}{\text{sign}[1 - a^2 y(m - 1)]^3}. \quad (43)$$

If we now require

$$\partial X_{\pm}^{\theta} / \partial m(m; q = q_{ex(\pm)}^{\theta}, y, a) = 0$$

somewhere at  $0 < m < 1$ , we obtain a condition

$$m > m_{d(ex)} \quad \text{for } y > 1/a^2,$$

which ensures

$$\frac{\partial^2 X_{\pm}^{\theta} / \partial m^2(m; q = q_{ex(\pm)}^{\theta}, y, a)}{a I^2} < 0. \quad (44)$$

Considering the previous results, we can conclude that the functions  $q_{ex(\pm)}^{\theta}(m; y, a^2)$  determine local maxima of the potential  $X_{\pm}^{\theta}(m; q, y, a)$  for  $q < -a^2$  that occur on this curve in the case  $y > 1/a^2$  in the interval  $m \in (m_{d(ex)}; 1)$ .

Proceeding the same way with the function  $X_{-}^{\theta}(m; q, y, a)$ , we first find that the equation

$$\partial X_{-}^{\theta} / \partial m(m; q = q_{ex(\pm)}^{\theta}, y, a) = 0$$

has always solution for some  $m \in (0; 1)$  in the case  $y < 1/a^2$ , but for  $y \geq 1/a^2$  this solution must fulfil  $m < m_{d(ex)}$ .

Substituting  $q = q_{ex(\pm)}^{\theta}$  into the second derivative of  $X_{-}^{\theta}(m; q, y, a)$  yields the same expression as that in (45), but now with the above conditions we have

$$\partial^2 X_{-}^{\theta} / \partial m^2(m; q = q_{ex(\pm)}^{\theta}, y, a) > 0,$$

indicating local minima. Therefore, the function  $q_{ex(\pm)}^{\theta}$  gives local minima of  $X_{-}^{\theta}(m; q, y, a)$  for  $y < 1/a^2$  at the whole interval  $m \in (0; 1)$ , and for  $y > 1/a^2$  at  $m \in (0; m_{d(ex)})$ .

In the special case  $y = 1/a^2$ , the function  $q_{ex(\pm)}^{\theta}$  reduces to the form

$$q_{ex(\pm)}^{\theta}(m; y = 1/a^2, a^2) = -a^2; \quad (45)$$

we can easily convince ourself that the function  $X_{-}^{\theta}$  has no local extremum in such case, and the extrema of  $X_{+}^{\theta}$  are given by the function  $q_{ex+}^{\theta}(m; y, a)$ .

The conditions (24), (27) ensuring the allowance of the latitudinal motion must be complemented by case when the functions  $X_{\pm}^{\theta}$  are not defined. Their definition range is given by relations (29), (30), but it can be shown that

the violation of the latter one imply  $M(m; X, q, y, a) > 0$ . In such case, the latitudinal motion is allowed for any impact parameter  $X$  (see the details in the discussion below). All characteristic functions are depicted in Fig. 1. and the graphs of the potentials in Fig. 2 for selected representative values of parameters.

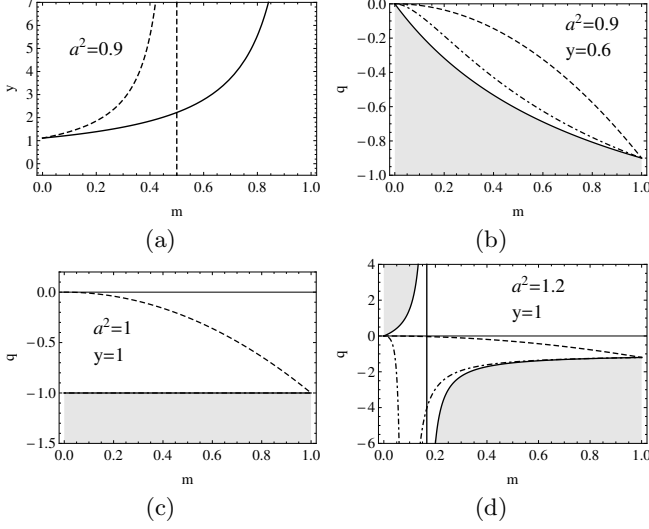


FIG. 1: The graphs of characteristic functions depicted for given parameters: **(a)**  $y_{d(r)}^\theta(m; a^2)$  (full curve) and  $y_{d(ex\pm)}^\theta(m; a^2)$  (dashed curve), the vertical line is the asymptote; **(b-d)**  $q_r^\theta(m; y, a^2)$  (full curve),  $q_{ex(+)}^\theta(m; a^2)$  (dashed curve),  $q_{ex(\pm)}^\theta(m; y, a^2)$  (dash-dotted curve) successively corresponding to cases  $y < 1/a^2$ ,  $y = 1/a^2$ ,  $y > 1/a^2$ . The unshaded region demarcates the definition range of the potentials  $X_\pm^\theta(m; q, y, a^2)$  given by conditions (29), (30).

Now we are able to discuss the behaviour of the potentials  $X_\pm^\theta(m; q, y, a)$  for various representative values of its parameters. The intersections of a line  $X = \text{const.}$  with the curves  $X_\pm^\theta(m; q, y, a)$  represents the turning points in variable  $m$ . From the knowledge of these functions we can thus get qualitative insight into the character of the latitudinal motion. This entitles us to following classification of Kerr-de Sitter spacetimes and brief description of the latitudinal motion. The basic division apparently consists of cases  $y < 1/a^2$ ,  $y = 1/a^2$ ,  $y > 1/a^2$ :

1. Case  $y < 1/a^2$

- $q < -a^2$ 
  - the definition range of the potentials is an empty set; the latitudinal motion is not possible;
- $q = -a^2$ 
  - the potentials  $X_\pm^\theta(m; q, y, a)$  are defined only for  $m = 1$ , where

$$X_+^\theta(1; q, y, a) = X_-^\theta(1; q, y, a) = -a;$$

photons with such values of parameters are the special case of the so called PNC

photons 'radially' moving along the spin axis [9];

- $-a^2 < q < 0$  (Fig. 2a, 2b)
  - both the potentials are defined for  $m \in \langle m_l; 1 \rangle$ , where the lower limit

$$m_l = \frac{q(a^2 y - 1)}{a^2(qy + 1)} > 0 \quad (46)$$

is the solution of the equation

$$q = q_r^\theta(m; y, a) \quad (\text{see Fig. 1b});$$

the limits of the interval are the common points of the potentials, where

$$X_\pm^\theta(m = m_l; q, y, a) = X_\pm^\theta(m_l) = \frac{a(1 + qy)}{a^2 y - 1} < 0; \quad (47)$$

- the latitudinal motion is allowed for values of the parameter  $X$  between some local minimum  $X_{\min(-)} = X_-^\theta(m_{\min(-)}; q, y, a)$  and maximum  $X_{\max(+)} = X_+^\theta(m_{\max(+)}; q, y, a)$ , for which

$$X_{\min(-)} < -a < X_{\max(+)} < 0;$$

the loci  $m_{\min(-)}$  of minimum  $X_{\min(-)}$  is given by the equation (39), the loci  $m_{\max(+)}$  of maximum  $X_{\max(+)}$  is determined by relation (37);

- if  $X$  takes one of these extremal values, then the trajectory of such photon lies entirely on cones  $\theta = \arccos \sqrt{m_{ex}}$ ,  $\theta = \pi - \arccos \sqrt{m_{ex}}$ , where  $m_{ex} \in \{m_{\min(-)}, m_{\max(+)}\}$ ; such photons are called PNC photons [9];
- for  $X_{\min(-)} < X < X_{\max(+)}$  there are two solutions  $m_1 < m_2$  of each of the two equations  $X = X_\pm(m; q, y, a)$ , implying that photon executes so called vortical motion, which is restricted between two pairs of cones, symmetrically placed relative to equatorial plane:

$$0 < \arccos \sqrt{m_2} \leq \theta \leq \arccos \sqrt{m_1} < \frac{\pi}{2}$$

and

$$\frac{\pi}{2} < \pi - \arccos \sqrt{m_1} \leq \theta \leq \pi - \arccos \sqrt{m_2} < \pi;$$

- in the special case  $X = -a$  one of the turning points is  $m_2 = 1$ , which represents transit through the spin axis; such photon therefore oscillate above one of the poles in cone which is delimited by the angle  $\theta = \arccos \sqrt{m_1}$ ;

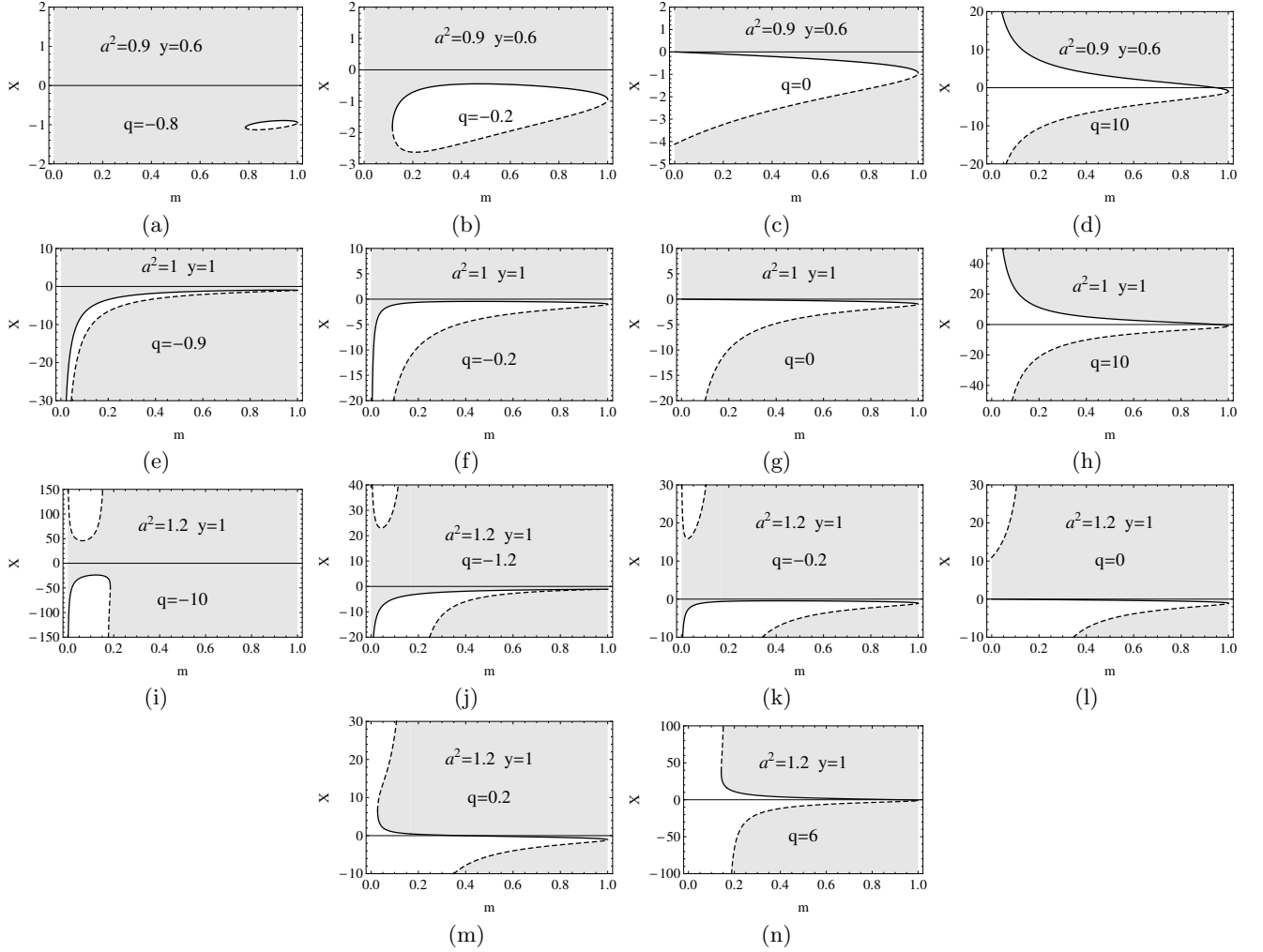


FIG. 2: Graphs of potentials  $X_+^\theta(m; q, y, a)$  (full curve) and  $X_-^\theta(m; q, y, a)$  (dashed curve) depicted for given typical values  $a^2, y$  corresponding successively to cases  $y < 1/a^2$  (top row),  $y = 1/a^2$  (middle row),  $y > 1/a^2$  (bottom row), and with  $q$  representing significant cases  $q < 0$ ,  $q = 0$ ,  $q > 0$ . Shading demarcates the region where the latitudinal motion is forbidden.

- from the preceding discussion it follows that we can expect that the case  $X = -a$  represents a change in azimuthal direction with respect to some privileged family of observers;
- $q = 0$  (Fig. 2c)
  - the expression in the definition (29) can be reduced to

$$X_\pm^\theta(m; y, a) = \frac{-a(1 \mp \sqrt{(1-m)\Delta_m})}{\Delta_m - a^2 y}, \quad (48)$$

which validity can be enlarged, without any repercussion on the correctness of the analysis, even for  $m = 0$ ; the definition range of the potentials is thus  $\langle 0; 1 \rangle$ ;

- from the equality  $W(\theta = \pi/2; X, q, y, a) = q$  it follows that at least in the equatorial plane the (radial) motion always exists for

$q = 0$ , where it can be both stable or unstable (see below); for  $q > 0$  the equatorial plane is crossed, for  $q < 0$  it can not be reached;

- there are no extrema of the potentials -  $X_+^\theta(m; q, y, a)$  is decreasing,  $X_-^\theta(m; q, y, a)$  is increasing; the permissible values of  $X$  for which  $d\theta/d\lambda > 0$  are still confined to an interval with limits

$$\begin{aligned} X_{min(-)}^\theta &= X_-^\theta(m=0; q=0, y, a) \\ &= \frac{2a}{(a^2 y - 1)} \end{aligned} \quad (49)$$

$$X_{max(+)}^\theta = X_+^\theta(m=0; q=0, y, a) = 0, \quad (50)$$

where  $X_{min(-)}^\theta < X_{max(+)}^\theta$ ;

- if  $X \leq X_{min(-)}^\theta$  or  $X \geq X_{max(+)}^\theta$  then the requirement  $W(\theta) \geq 0$  is fulfilled only if

$\theta = \pi/2$ , and in such case  $d\theta/d\lambda = 0$ , thus the motion is stably confined to the equatorial plane;

- for  $X_{min(-)}^\theta < X < X_{max(+)}^\theta$  photon initially released in the direction off the equatorial plane is once reflected at  $\theta = \arccos \sqrt{m_0}$  or  $\theta = \pi - \arccos \sqrt{m_0}$  respectively, where  $m_0$  denotes the only solution of  $X = X_\pm^\theta(m; q, y, a)$ ; another point where  $d\theta/d\lambda = 0$  is now in the equatorial plane, however the equality  $d^2\theta/d\lambda^2 = 0$  implies halting in the latitudinal direction; the function  $W(\theta)$  has at  $\theta = \pi/2$  local minimum, which indicates, as follows from perturbation analysis, instability in the equatorial plane;
- if specially  $X = -a$  then  $m_0 = 1$ , thus photon initially directed off the equatorial plane crosses the spin axis and finally is captured in the equatorial plane;
- $q > 0$  (Fig. 2d)
  - the potentials are defined for  $m \in (0, 1)$ ; they are monotonous in the same manner as in the case  $q = 0$ , but  $X_+^\theta(m; q, a, y) \rightarrow +\infty$  and  $X_-^\theta(m; q, y, a) \rightarrow -\infty$  as  $m \rightarrow 0$ ;
  - from the behaviour of the potentials it follows that for  $X \neq -a$  photon is forced to oscillate in  $\theta$ -direction through the equatorial plane between two cones governed by  $\arccos \sqrt{m_0} \leq \theta \leq \pi - \arccos \sqrt{m_0}$ , with  $m_0$  of the same meaning as above;
  - case  $X = -a$  represents the motion above both poles;
  - the foregoing conclusion is a reason to have a suspicion that cases  $X < -a$  and  $X > -a$  differ in the azimuthal direction relative to some family of stationary observers, it corresponds to  $\ell > 0$  and  $\ell < 0$ ;

## 2. Case $y = 1/a^2$

- the potentials simplify into the form

$$X_\pm^\theta(m; q, a) = \frac{-a \pm \sqrt{(1-m^2)(q+a^2)}}{m}; \quad (51)$$

- $q < -a^2$ 
  - the potentials are not defined, thus the latitudinal motion is not allowed;
- $q = -a^2$ 
  - the curves  $X = X_\pm^\theta(m; q = -a^2, y = 1/a^2, a)$  coalesce, since

$$\begin{aligned} X_+^\theta(m; q = -a^2, y = 1/a^2, a) &= \\ X_-^\theta(m; q = -a^2, y = 1/a^2, a) &= X_{(\pm)}^\theta(m; a) \equiv \frac{-a}{m}; \end{aligned} \quad (52)$$

- for  $X \leq -a$  there is one solution of the equation  $X = X_{(\pm)}^\theta(m; a)$ , which gives  $m = m_{(\pm)} \equiv -a/X$ ; this corresponds to PNC photons moving along cones  $\theta = \arccos \sqrt{m_{(\pm)}}$ ,  $\theta = \pi - \arccos \sqrt{m_{(\pm)}}$ ;
- for  $X \rightarrow -\infty$  the cones approach the equatorial plane;
- if specially  $X = -a$  the cones degenerate to spin axis, therefore, such PNC photons move along the spin axis;
- for  $X > -a$  there is no motion allowed;
- $-a^2 < q < 0$  (Fig. 2e, 2f)
  - the potentials are both defined for  $m \in (0, 1)$ ; there is one local maximum  $X_{max(+)}^\theta$  given by (37) of the function  $X_+^\theta(m; q, y, a)$  and no extremum of  $X_-^\theta(m; q, y, a)$ ; it holds  $X_-^\theta(m; q, y, a) < X_+^\theta(m; q, y, a) < 0$  and  $X_-^\theta(m; q, y, a), X_+^\theta(m; q, y, a) \rightarrow -\infty$  as  $m \rightarrow 0$  from the right;
  - if  $X < -a$  or  $-a < X < X_{max(+)}^\theta$ , the vortical motion exists;
  - for  $X = -a$  the 'inner' cones coalesce with the spin axis, thus the vortical motion involves crossing the poles;
  - for  $X = X_{max(+)}^\theta$  both the 'inner' and 'outer' cones coalesce, giving thus rise to PNC photons;
  - if  $X > X_{max(+)}^\theta$ , no motion is allowed;
- $q = 0$  (Fig. 2g)
  - the same discussion holds as in the case  $y < 1/a^2$ , except that the motion exists for  $X$  arbitrarily small;
- $q > 0$  (Fig. 2h)
  - the same conclusions holds as in the case  $y < 1/a^2$ ;

## 3. Case $y > 1/a^2$

- $q < -a^2$  (Fig. 2i)
  - the definition range of both potentials is an interval  $(0; m_u)$  (see the purple curve in Fig. 1d), where the upper limit  $m_u < 1$  is given as  $m_l$  in the previous case by (46);
  - there is  $X_+^\theta(m; q, y, a) \rightarrow -\infty$  and  $X_-^\theta(m; q, y, a) \rightarrow +\infty$  as  $m \rightarrow 0$ , moreover,  $X_-^\theta(m; q, y, a)$  now diverge at  $m = m_d$ , which is the solution of (33), and  $X_-^\theta(m; q, y, a) \rightarrow +\infty (-\infty)$  as  $m \rightarrow m_d$  from the left (right);
  - there are thus two regions of permissible values  $X$  in the  $(m, X)$ -plane for which the motion can exist; the lower one bounded by the graph of  $X_+^\theta$  and the lower branch



of  $X_-^\theta$ , which at  $m = m_u$  join into continuous curve, and the upper region given by the upper branch of  $X_-^\theta$ ; the motion is therefore allowed for  $X \leq X_{max(+)}^\theta < -a$  or  $X \geq X_{min(-)}^\theta > 0$ , where the loci of local extrema  $X_{max(+)}^\theta, X_{min(-)}^\theta$  are given by (39) (see the blue curve in Fig. 1d);

- if  $X < X_{max(+)}^\theta$  or  $X > X_{min(-)}^\theta$  photon executes vortical motion, cases  $X = X_{max(+)}^\theta, X = X_{min(-)}^\theta$  correspond to PNC photons;
- for  $X = X_-^\theta(m_u) = X_+^\theta(m_u) = a(1 + qy)/(a^2y - 1)$ , the inner cones delimiting the vortical motion are the narrowest;
- for  $X \rightarrow -\infty$  or  $X \rightarrow +\infty$  the outer cones given by angles

$$\theta = \arccos \sqrt{m_1}, \quad \theta = \pi - \arccos \sqrt{m_1}$$

approach the equatorial plane since  $m_1 \rightarrow 0$ ; for the inner cones

$$\theta = \arccos \sqrt{m_2}, \quad \theta = \pi - \arccos \sqrt{m_2},$$

there is

$$m_2 \rightarrow m_d = 1 - 1/a^2 y;$$

- $q = -a^2$  (Fig. 2j)
  - there is no local extremum of the function  $X_+^\theta(m; q, y, a)$ , which is now increasing; it holds  $m_u = 1, X_-^\theta(m_u) = X_+^\theta(m_u) = X_{+(max)}^\theta = -a$ , hence for  $X = -a$  both the inner and outer cones coalesce with the spin axis, which again corresponds to 'axial' PNC photon;
  - another PNC photons exist for  $X = X_{min(-)}^\theta > 0$ ;
  - there are no other qualitative differences from the case  $q < -a^2$ ;
- $-a^2 < q < 0$  (Fig. 2k)
  - the definition range is an interval  $(0; 1)$  and the divergencies of the potentials are the same as above;
  - the function  $X_+^\theta(m; q, y, a)$  has now local maximum  $X_{max(+)}^\theta, -a < X_{max(+)}^\theta < 0, X_{max(+)}^\theta \rightarrow 0$  for  $q \rightarrow 0$ , determined by equation (37);
  - case  $X = -a$  now corresponds to vortical motion above the poles - the inner cones have coalesced with the spin axis, the outer ones stay open;
  - the vortical motion exists as in the previous cases and above that for  $-a < X < X_{max(+)}^\theta$ ;

- $q = 0$  (Fig. 2l)
  - the definition (48) holds, the functions  $X_{+(-)}^\theta(m; q, y, a)$  are defined at  $\langle 0, 1 \rangle \setminus \langle 0, 1 \rangle \setminus \{m_d\}$ ; the values for  $m = 0$  are given by (50), but now  $X_{max(+)}^\theta < X_{min(-)}^\theta$ ;
  - the potential  $X_+^\theta(m; y, a)$  is decreasing in its whole definition range,  $X_-^\theta(m; y, a)$  is piecewise increasing because of the divergent point  $m_d$ ;
  - if  $X \leq X_{max(+)}^\theta = 0$  or  $X \geq X_{min(-)}^\theta$  then the same conclusions can be made as in the case  $y < 1/a^2$  for  $X_{min(-)}^\theta \leq X \leq X_{max(+)}^\theta$ ;
  - for  $X_{max(+)}^\theta < X < X_{min(-)}^\theta$  it holds  $W(\theta = \pi/2; X, q = 0, y, a) = 0$  again, otherwise  $W(\theta; X, q = 0, y, a) < 0$ , therefore photons can radially move in the equatorial plane;
- $q > 0$  (Fig. 2m, 2n)
  - the function  $X_+^\theta(m; q, y, a)$  is defined at  $\langle m_l, 1 \rangle$ , the function  $X_-^\theta(m; q, y, a)$  at  $\langle m_l, 1 \rangle \setminus \{m_d\}$ , where  $m_l$  is given by (46) with the difference that now  $X_{(\pm)}^\theta(m_l) > 0$ ; the graphs of both functions now form a single open curve, which intersects a line  $X = \text{const.}$  at a single point;
  - in the interval  $m \in \langle 0; m_l \rangle$  the latitudinal motion is allowed for arbitrarily large or small value of the motion constant  $X$ ;
  - for arbitrary  $X \neq -a$  there exists oscillatory motion through the equatorial plane as described in the case  $y < 1/a^2, q > 0$ ;
  - if  $X = X_{(\pm)}^\theta(m_l)$  the boundary cones are closest to equatorial plane, they are given by angles

$$\theta = \arccos \sqrt{m_l}, \quad \theta = \pi - \arccos \sqrt{m_l};$$

- the case  $X = -a$  corresponds to orbits above both poles crossing also the equatorial plane;
- there is no vortical motion or PNC photons;

We finish this section with setting the allowed region in the  $(X, q)$ -plane delimiting such combinations of the motion constants, for which the latitudinal motion is possible, in dependence on the spacetime parameters  $a, y$ .

From the requirement that the function  $M(m; a, y, X, q)$  defined in the relation (22) has to be non-negative somewhere in the interval  $m \in \langle 0; 1 \rangle$ , one can derive that the allowed region of the  $(X - q)$ -plane is determined by the condition

$$q \geq q_{min}(X, y, a), \quad (53)$$

where  $q_{min}(X, y, a)$  is defined using functions

$$q_1(X) \equiv -X^2 \quad (54)$$

and

$$q_2(X; y, a) \equiv -I^{-2}[(1 - a^2 y)X + 2a]^2 \quad (55)$$

as follows (see Fig. 3 and Fig. 4):

- Case  $y < 1/a^2$  (Fig. 3a)

$$q_{min}(X, y, a) \equiv \begin{cases} 0, & \text{for } X < \frac{2a}{a^2 y - 1} \text{ or } X > 0; \\ q_2(X; y, a), & \text{for } \frac{2a}{a^2 y - 1} \leq X < -a; \\ q_1(X), & \text{for } -a \leq X \leq 0; \end{cases} \quad (56)$$

- Case  $y = 1/a^2$  (Fig. 3b)

$$q_{min}(X, y, a) \equiv \begin{cases} -a^2, & \text{for } X \leq -a; \\ q_1(X), & \text{for } -a \leq X \leq 0; \\ 0, & \text{for } X \geq 0; \end{cases} \quad (57)$$

- Case  $y > 1/a^2$  (Fig. 3c)

$$q_{min}(X, y, a) \equiv \begin{cases} q_2(X; y, a), & \text{for } X < -a \\ & \text{or } \frac{2a}{a^2 y - 1} < X; \\ q_1(X), & \text{for } -a \leq X \leq 0; \\ 0, & \text{when } 0 < X \leq \frac{2a}{a^2 y - 1}; \end{cases} \quad (58)$$

The case  $y < 1/a^2$  qualitatively corresponds to both black hole and naked singularity spacetimes, the other two cases  $y = 1/a^2$  and  $y > 1/a^2$  describe the naked singularity spacetimes (see Fig. 7 in the next section). The  $q = \text{const.}$  slices of the function  $q_{min}(X, y, a)$  give for  $q < 0$  extremal values  $X_{min(-)}$ ,  $X_{max(+)}$  of the potentials  $X_{\pm}^{\theta}(m; q, y, a)$  discussed in the text.

#### IV. RADIAL MOTION

From the equation (14) it is clear that the radial motion can exist if  $R(r) \geq 0$ , where the equality gives the turning points of the radial motion. This condition can be rewritten in terms of an ‘effective potential’  $X_{\pm}$  in the form

$$X \leq X_- \text{ or } X \geq X_+, \quad (59)$$

if

$$a^2 - \Delta_r > 0 \quad (\text{and } X_- < X_+),$$

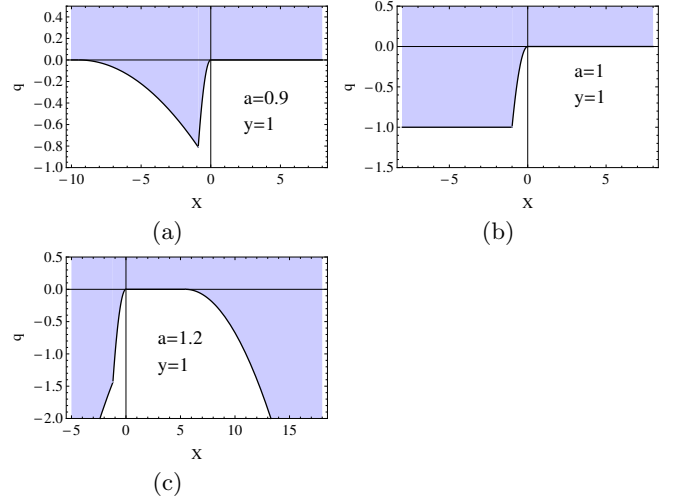


FIG. 3: The allowed region in the motion constant plane ( $X - q$ ) depicted for some representative values of space-time parameters  $a, y$ , successively corresponding to cases  $y < 1/a^2$ ,  $y = 1/a^2$ ,  $y > 1/a^2$ . An intersections of a line  $q = \text{const.} < 0$  with the border curves  $q_1(X)$ ,  $q_2(X; y, a)$  determines the extremal values  $X_{min(-)}$ ,  $X_{max(+)}$  of the potentials  $X_{\pm}^{\theta}(m; q, y, a)$  introduced in the discussion above.

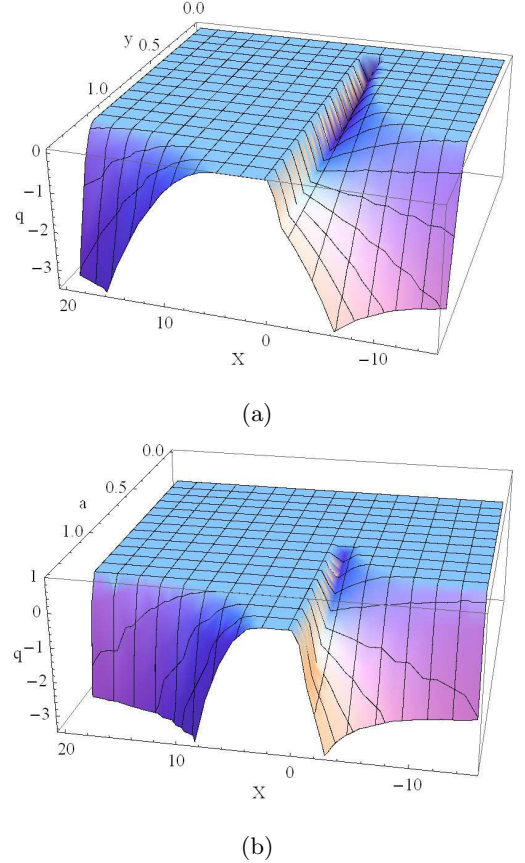


FIG. 4: Parameter spaces ( $q - X - y$ ) for  $a = 1$  (a), and ( $q - X - a$ ) for  $y = 1$  (b) divided by separating surface in two sub-spaces corresponding to allowed (above) and forbidden (beneath) values of kinetic constants  $q, X$ .

or

$$X_+ \leq X \leq X_- \quad \text{if} \quad a^2 - \Delta_r < 0, \quad (60)$$

where

$$X_{\pm}(r; q, y, a) \equiv \frac{ar^2 \pm \sqrt{\Delta_r [r^4 + q(a^2 - \Delta_r)]}}{a^2 - \Delta_r}. \quad (61)$$

We start the analysis by determining the reality region of the effective potential  $X_{\pm}$ . From the expression (61) it follows that this function is well defined for

$$q \begin{cases} \leq q_r(r; y, a^2) & \text{if } a^2 < \Delta_r \text{ or } \Delta_r \leq 0 \\ \geq q_r(r; y, a^2) & \text{if } 0 \leq \Delta_r < a^2 \end{cases}, \quad (62)$$

where we have introduced the reality function

$$q_r(r; y, a^2) \equiv \frac{r^4}{\Delta_r - a^2} = \frac{r^3}{r - 2 - yr(r^2 + a^2)}. \quad (63)$$

There are thus two different types of the boundary points of the definition range of  $X_{\pm}(r; q, a, y)$ . The points of the first type lie stably for given spacetime parameters on the borders of the static regions determined by the relation 9, i. e. at the event horizons ( $r = r_h$ ). At these horizons, if they exist, for arbitrary parameter  $q$ , the functions  $X_{\pm}$  have common values

$$X_+(r_h) = X_-(r_h) = \frac{r_h^2}{a} \quad (64)$$

(c. f. [66]). The points of the second type, which are also common points of  $X_{\pm}$ , depend on the value of parameter  $q$  and are given by the equality  $q = q_r(r; y, a^2)$ . If we denote them  $r = r_q$  then it holds

$$X_+(r_q) = X_-(r_q) = -\frac{aq}{r_q^2}. \quad (65)$$

The divergencies of the function  $q_r(r; y, a^2)$ , which are incident with divergent points of  $X_+(r; q, y, a)$ , are located at radii where

$$\Delta_r = a^2, \quad (66)$$

which one can express by the relation

$$y = y_d(r; a^2) \equiv \frac{r - 2}{r(r^2 + a^2)}. \quad (67)$$

The function  $X_-(r; q, y, a)$  can not diverge at radii  $r_d$  given by (66), since using an alternative expression

$$X_{\pm}(r; q, y, a) \equiv \frac{r^4 - q\Delta_r}{ar^2 \mp \sqrt{\Delta_r [r^4 + q(a^2 - \Delta_r)]}} \quad (68)$$

it can be shown that it has finite value

$$X_-(r_d; q, y, a) = \frac{r_d^4 - qa^2}{2ar_d^2}. \quad (69)$$

Another point where the functions  $X_{\pm}(r; q, y, a)$  diverge is  $r = 0$ , with  $X_{\pm}(r; q, y, a) \rightarrow \pm\infty$  as  $r \rightarrow 0$  for  $q > 0$ , but for  $q = 0$  it holds  $X_{\pm}(r; q = 0, y, a) \rightarrow 0$ .

The character of the function  $y_d(r; a^2)$  has been discussed in [63, 66], therefore we briefly repeat that the only zero of  $y_d(r; a^2)$  is at  $r = 2$ , the extrema, which for  $a^2 > 0$  must be maxima, yields the relation

$$a^2 = a_{max(d)}^2(r) \equiv r^2(r - 3). \quad (70)$$

The only zero of  $q_r(r; y, a^2)$  is at  $r = 0$ . For  $r \rightarrow \infty$  it holds  $q_r(r; y, a) \rightarrow -1/y$ . Its extrema are determined by

$$y = y_{ex(r)}(r; a^2) \equiv \frac{r - 3}{a^2 r}. \quad (71)$$

The divergency of  $y_{ex(r)}(r; a^2)$  is at  $r = 0$  and  $y_{ex(r)}(r; a^2) \rightarrow -\infty$  for  $r \rightarrow 0$ . For  $r \rightarrow \infty$  it approaches the line  $1/a^2$  from below. The zero is at  $r = 3$  and its extrema do not exist, the function is purely increasing.

Now we shall specify the local extrema of the effective potential, which determine the radii of spherical photon orbits. They are given by the condition  $\partial X_{\pm}/\partial r = 0$ , which implies

$$r^4 + a^2 q = 0, \quad (72)$$

or

$$q a^2 [2yr^3 + (ya^2 - 1)r + 1]^2 + r^3 [y^2 a^4 r^3 + 2ya^2 r^2(r + 3) + r(r - 3)^2 - 4a^2] = 0. \quad (73)$$

This can be rewritten in terms of parameter  $q$  as

$$q = q_{ex1}(r; a^2) \equiv -\frac{r^4}{a^2}, \quad (74)$$

and

$$q = q_{ex}(r; y, a^2) \equiv -\frac{r^3}{a^2} \frac{y^2 a^4 r^3 + 2ya^2 r^2(r + 3) + r(r - 3)^2 - 4a^2}{[2yr^3 + (ya^2 - 1)r + 1]^2}. \quad (75)$$

Note that the function  $q_{ex1}(r; a^2)$  is independent of the cosmological parameter. Both the functions  $q_{ex1}(r; a^2)$ ,  $q_{ex}(r; y, a^2)$  have common points determined by

$$y = \frac{r^2 - 2r + a^2}{r^2(r^2 + a^2)} = y_h(r; a^2), \quad (76)$$

and

$$y = \frac{1}{r^3}, \quad (77)$$

i. e., they are located at event horizons and so called static radius  $r_s = 1/\sqrt[3]{y}$ , where the gravitational attraction is just compensated by cosmological repulsion [59, 65]. The function  $q_{ex1}(r; a^2)$  is negative valued and

hence, as we shall see bellow, the extrema of the potentials  $X_{\pm}$  determined by this function lie in regions forbidden by conditions for the reality of latitudinal motion. The divergencies of  $q_{ex}(r; y, a^2)$  are determined by the relation

$$y = y_{d(ex)}(r; a^2) \equiv \frac{r-1}{r(2r^2+a^2)}, \quad (78)$$

its asymptotic behaviour is given by  $q_{ex}(r; y, a^2) \rightarrow -(I/2ay)^2$  as  $r \rightarrow \infty$ .

The function  $y_{d(ex)}(r; a^2)$  diverges for  $r = 0$  and  $y_{d(ex)}(r; a^2) \rightarrow -\infty$  as  $r \rightarrow 0$ . For  $r \rightarrow \infty$  it holds  $y_{d(ex)}(r; a^2) \rightarrow 0$ . The zero of this function is at  $r = 1$  and its local extrema are determined by the relation

$$a^2 = a_{max(d(ex))}^2(r) \equiv 2r^2(2r-3), \quad (79)$$

where the label 'max' indicates that at relevant range  $r \geq 3/2$ , these extrema must be maxima.

The zero point of the function  $q_{ex}(r; y, a^2)$  is at  $r = 0$ , another zeros determine the loci of the circular equatorial photon orbits. They are given by the relation

$$y = y_{z(ex)\pm}(r; a^2) \equiv \frac{-r(r+3) \pm 2\sqrt{r(3r^2+a^2)}}{a^2 r^2}. \quad (80)$$

Since the function  $y_{z(ex)-}(r; a^2) < 0$  for  $r > 0$ , it is irrelevant in our discussion. The function  $y_{z(ex)+}(r; a^2)$  is real valued for all  $r > 0$  and it diverges at  $r = 0$ , with  $y_{z(ex)+}(r; a^2) \rightarrow \infty$  as  $r \rightarrow 0$ . For  $r \rightarrow \infty$ , we find  $y_{z(ex)+}(r; a^2) \rightarrow -1/a^2$ . Its zeros represent the equatorial circular photon orbits in the Kerr spacetimes, being determined by the relation [58]

$$a^2 = a_{z(ex)+}^2(r) \equiv \frac{r(r-3)^2}{4}. \quad (81)$$

The extrema of the function  $y_{z(ex)+}(r; a^2)$  are determined by the equation

$$a^2 = a_{ex(z(ex)+)\pm}^2(r) \equiv \frac{r(1-2r \pm \sqrt{1+8r})}{2} = a_{ex(h)\pm}^2(r), \quad (82)$$

hence the loci of extrema of the functions  $y_{z(ex)+}(r; a^2)$  and  $y_h(r; a^2)$  coalesce.

The function  $a_{ex(z(ex)+)-}^2(r)$  should be excluded from further analysis since for  $r > 0$  there is  $a_{ex(z(ex)+)-}^2(r) < 0$ .

It remains to determine loci of the local extrema of the function  $q_{ex}(r; y, a^2)$ . Proceeding the usual way we find that their occurrence is governed by the relations

$$y = y_{ex(ex)}(r; a^2) \equiv \frac{r-3}{a^2 r} = y_{ex(r)}(r; a^2) \quad (83)$$

and

$$y = y_{ex(ex)\pm}(r; a^2) \equiv$$

$$\frac{3r^2\sqrt{r} - a^2\sqrt{r}(3+2r) \pm \sqrt{(4a^2-3r)(a^4+6a^2r^2-3r^4)}}{2a^4\sqrt{r^3}}. \quad (84)$$

Using the relation (83), one can show that the extrema of both functions  $q_{ex}(r; y, a^2)$ ,  $q_r(r; y, a^2)$  coalesce. At this point let us add that another common points of functions  $q_{ex}(r; y, a^2)$ ,  $q_r(r; y, a^2)$ , as well as of the functions  $q_{ex1}(r; y, a^2)$ ,  $q_r(r; y, a^2)$ , are also given by

$$y = y_h(r; a^2), \quad (85)$$

i. e. they are located at the event horizons.

The reality conditions of the functions  $y_{ex(ex)\pm}(r; a^2)$  read

$$a^2 \leq a_{r(ex(ex)\pm)+}^2(r) \quad \text{or} \quad a_{r(ex(ex)\pm)}^2(r) \leq a^2, \quad (86)$$

$$\text{if } 0 < r \leq \hat{r},$$

and

$$a^2 \leq a_{r(ex(ex)\pm)}^2(r) \quad \text{or} \quad a_{r(ex(ex)\pm)+}^2(r) \leq a^2, \quad (87)$$

$$\text{if } \hat{r} \leq r,$$

where

$$a_{r(ex(ex)\pm)+}^2(r) \equiv (+2\sqrt{3}-3)r^2 \quad (88)$$

and

$$a_{r(ex(ex)\pm)}^2(r) \equiv \frac{3}{4}r. \quad (89)$$

The marginal radius  $\hat{r}$  has value

$$\hat{r} = \frac{2\sqrt{3}+3}{4} = 1.61603 = r_{crit} \quad (90)$$

and it holds

$$a_{r(ex(ex)\pm)+}^2(\hat{r}) = a_{r(ex(ex)\pm)}^2(\hat{r}) = a_{crit}^2 = 1.21202, \quad (91)$$

where  $a_{crit}^2$  corresponds to local maximum of the function  $a_{ex(h)+}^2(r)$  (see e. g. [66] for details).

The functions  $y_{ex(ex)\pm}(r; a^2)$  have the divergency point at  $r = 0$  and  $y_{ex(ex)\pm}(r; a^2) \rightarrow \pm\infty$  for  $r \rightarrow 0$ . For  $r \rightarrow \infty$  we find that  $y_{ex(ex)+}(r; a^2) \rightarrow \infty$  and  $y_{ex(ex)-}(r; a^2) \rightarrow 0$  from above.

The zero point of  $y_{ex(ex)}(r; a^2)$  is at  $r = 3$  and the function is increasing for all  $r > 0$ .

Zeros of the functions  $y_{ex(ex)\pm}(r; a^2)$  are given by

$$a^2 = a_{z(ex(ex)\pm)}^2(r) \equiv r(r^2-3r+3). \quad (92)$$

The condition for stationary points

$$\partial y_{ex(ex)\pm}(r; a^2)/\partial r = 0$$

leads to

$$a^4 + a^2 r(2r-1) + r^3(r-3) = 0,$$

which can be solved with respect to  $a^2$  with the same result as given by (12). However, substitution into the second derivative concurrently with the requirement  $y_{ex(ex)\pm}(r; a^2) > 0$  implies

$$\partial^2 y_{ex(ex)\pm}(r; a^2 = a_{ex(h)+}^2(r)) = 0, \quad (93)$$

therefore the function

$$a_{inf(ex(ex)\pm)+}^2(r) \equiv a_{ex(h)+}^2(r) \quad (94)$$

determines the loci of the inflex points of the functions  $y_{ex(ex)\pm}(r; a^2)$ .

If we compare the asymptotic behaviour of all characteristic functions  $y(r; a^2)$ , we find that following inequality is satisfied:

$1/a^2 > y_{ex(ex)}(r; a^2) > y_{ex(ex)-}(r; a^2) > y_h(r; a^2) > y_d(r; a^2) > y_{d(ex)}(r; a^2) > 0 > y_{z(ex)}(r; a^2) > -1/a^2$  as  $r \rightarrow \infty$ .

In Fig.5 we present all the characteristic functions related to spin parameter governing the effective potential on the lowest level:

- $a_{z(h)}^2(r)$
- $a_{ex(h)+}^2(r) = a_{ex(z(ex))+}^2(r) = a_{inf(ex(ex)\pm)+}^2(r)$
- $a_{max(d)}^2(r)$
- $a_{max(d(ex))}^2(r)$
- $a_{z(z(ex)+)}^2(r)$
- $a_{r(ex(ex)\pm)+}^2(r)$
- $a_{r(ex(ex)\pm)}^2(r)$
- $a_{z(ex(ex)\pm)}^2(r)$ .

These functions determine the behaviour of the characteristic functions related to the cosmological parameter, characterizing the functions  $q(r; y, a^2)$  and then effective potentials on the higher level:

- $y_h(r; a^2)$
- $y_d(r; a^2)$
- $y_{ex(r)}(r; a^2) = y_{ex(ex)}(r; a^2)$
- $y_{d(ex)}(r; a^2)$
- $y_{z(ex)+}(r; a^2)$
- $y_{ex(ex)\pm}(r; a^2)$ .

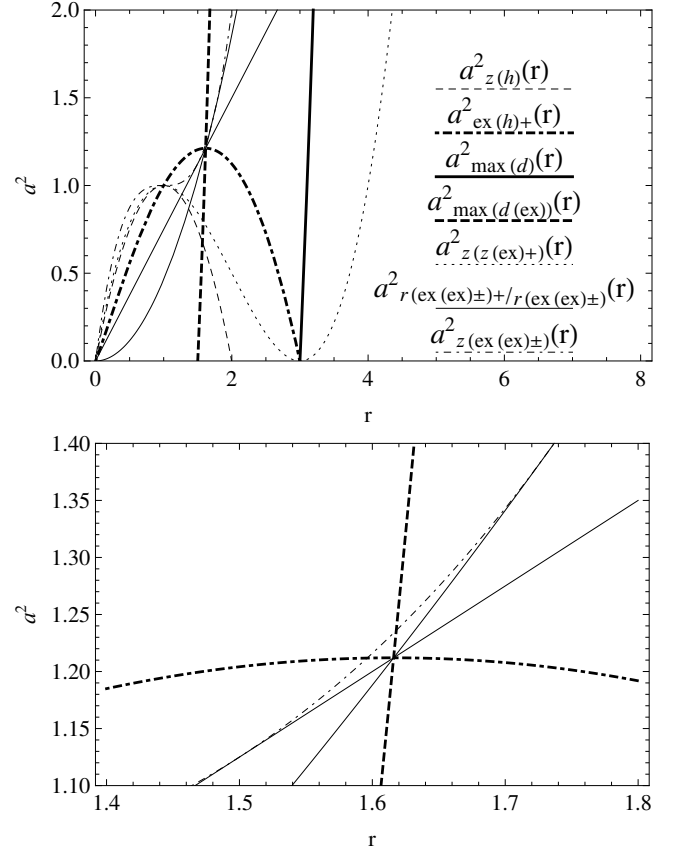


FIG. 5: Characteristic functions  $a^2(r)$  determining the behaviour of functions the  $y(r; a^2)$ .

From the significance of the individual characteristic functions  $a^2(r)$  depicted in Fig. 5, one can infer that there are just two values of  $a^2$  being of particular importance and leading to qualitatively different behaviour of the functions  $y(r; a^2)$ :

$a^2 = 1$  – the common local maximum of the functions  $a_{z(h)}^2(r)$  and  $a_{z(z(ex))}^2(r)$  at  $r = 1$ , which coincides with the inflection point of the function  $a_{z(ex(ex)\pm)}^2(r; a^2)$  and with the intersection with the curve  $a_{ex(h)+}^2(r)$

$a^2 = a_{crit}^2 = 1.21202$  – the local maximum  $a_{ex(h)+}^2(r)$  which is the intersection of the curves  $a_{r(ex(ex)\pm)+}^2(r)$ ,  $a_{r(ex(ex)\pm)}^2(r)$  and  $a_{max(d(ex))}^2(r)$ .

The graphs of characteristic functions  $y(r; a^2)$  depicted for some values of spin parameter  $a$  representing cases  $0 < a^2 < 1$ ,  $1 < a^2 < a_{crit}^2$  and  $a_{crit}^2 < a^2$  are presented in Fig. 6.

In general, behaviour of the characteristic functions  $q_r(r; y, a^2)$  and  $q_{ex}(r; y, a^2)$  will be qualitatively different, if for the parameter  $a$  we being fixed take the  $y$ -values from different intervals, which are limited by intersections and/or extrema of the characteristic functions  $y(r; a^2)$  that are demonstrated in Fig. 6. We therefore need to determine curves  $y(a^2)$  that separate the

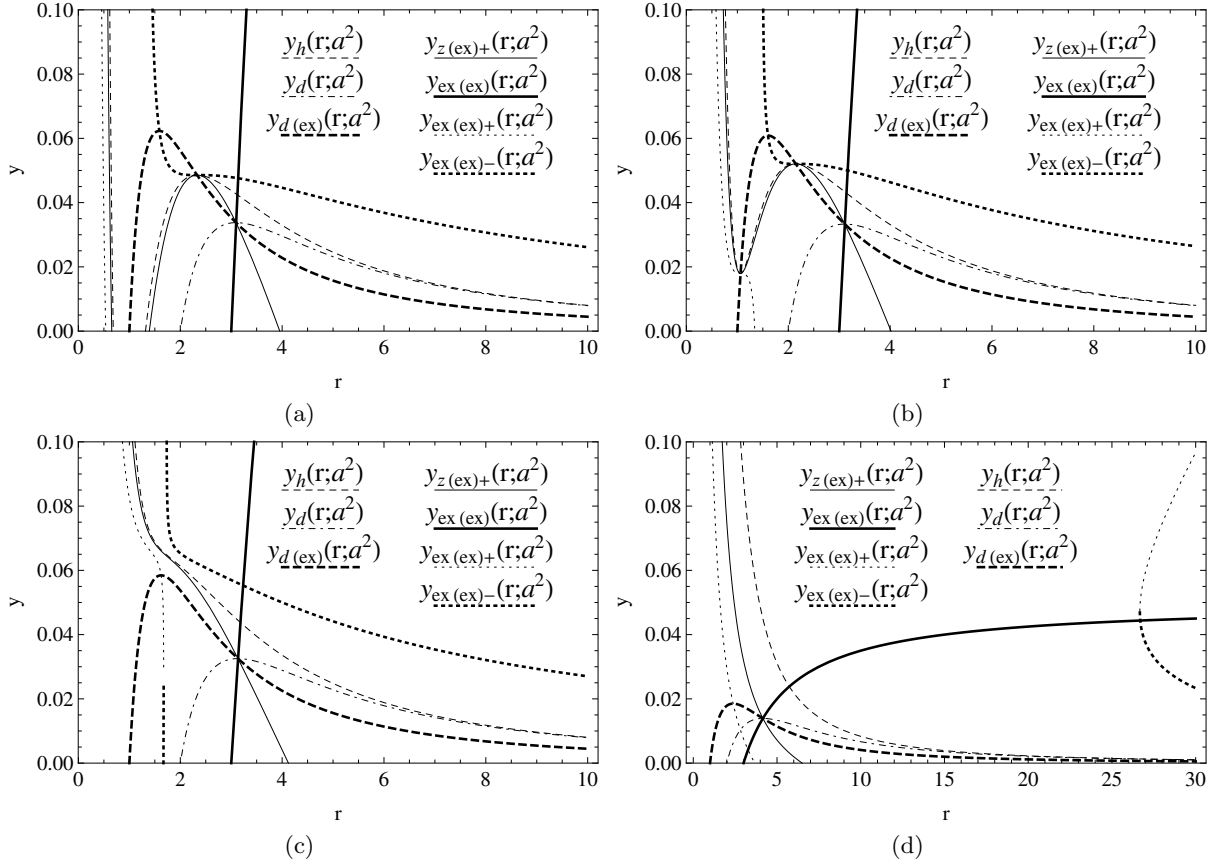


FIG. 6: Characteristic functions  $y(r; a^2)$  given for  $a^2 = 0.9$  (a),  $a^2 = 1.04$  (b),  $a^2 = 1.3$  (c) and  $a^2 = 20$  (d).

$(a^2-y)$ -plane into regions that correspond to that different behaviour of the characteristic functions  $q_r(r; y, a^2)$  and  $q_{ex}(r; y, a^2)$ . The number of these functions is substantially lowered by the fact that all the local extrema are multiple intersections with other curves and coincide with other extrema. The functions that we need can be ordered according to their importance as follows:

- $y_{max(h)}(a^2) = y_{max(z(ex)+)}(a^2) = y_{inf(ex(ex)-)}(a^2) = y_{d(ex)-h-(z(ex)+)-ex(ex)-}(a^2)$
- $y_{min(h)}(a^2) = y_{min(z(ex)+)}(a^2) = y_{inf(ex(ex)+)}(a^2) = y_{d(ex)-h-(z(ex)+)-ex(ex)+}(a^2)$
- $y_{max(d)}(a^2) = y_{d-d(ex)-(z(ex)+)-ex(ex)}(a^2)$
- $y_{d-(z(ex)+)}(a^2)$
- $y_{max(d(ex))}(a^2) = y_{d(ex)-ex(ex)-}(a^2)$
- $y_{ex(ex)-(ex(ex)+)}(a^2)$
- $y_{d-(ex(ex)+)}(a^2)$
- $y_{ex(ex)-h}(a^2)$
- $y_{ex(ex)-(ex(ex)-)}(a^2)$

Here the dashes between two labels denote affiliation to intersection of appropriate functions (it can be proved that there are no other intersections of these functions than that shown in Fig.6). These functions are projections of extremal values or intersections of characteristic functions  $y(r; a^2)$  into  $(a^2-y)$ -plane and they are demonstrated in Fig. 7.

The functions  $y_{ex(h)}(a^2)$  divide the parameter plane  $(a^2-y)$  into regions describing Kerr-de Sitter black hole and naked singularity spacetimes, the curve  $y_{max(d)}(a^2)$  represents additional division of spacetimes with so called divergent and restricted repulsive barrier of photon motion. A detailed discussion of these functions have been performed e. g. in [66, 78] and will not be repeated here. The significance of the remaining functions can be understood from the depiction of the characteristic functions  $q_r(r; y, a^2)$ ,  $q_{ex}(r; y, a^2)$  in Fig 8. They are given parametrically by appropriate functions  $a^2(r)$ ,  $y(r; a^2(r))$  with  $r$  being the parameter:

- the functions  $y_{max(h)}(a^2)$  and  $y_{min(h)}(a^2)$  are both determined by  $a^2_{ex(h)+}(r)$  and  $y_h(r; a^2 = a^2_{ex(h)+}(r))$ ;
- $y_{max(d)}(a^2)$  we obtain from  $a^2_{max(d)}(r)$  with  $y_d(r; a^2 = a^2_{max(d)}(r))$ ;

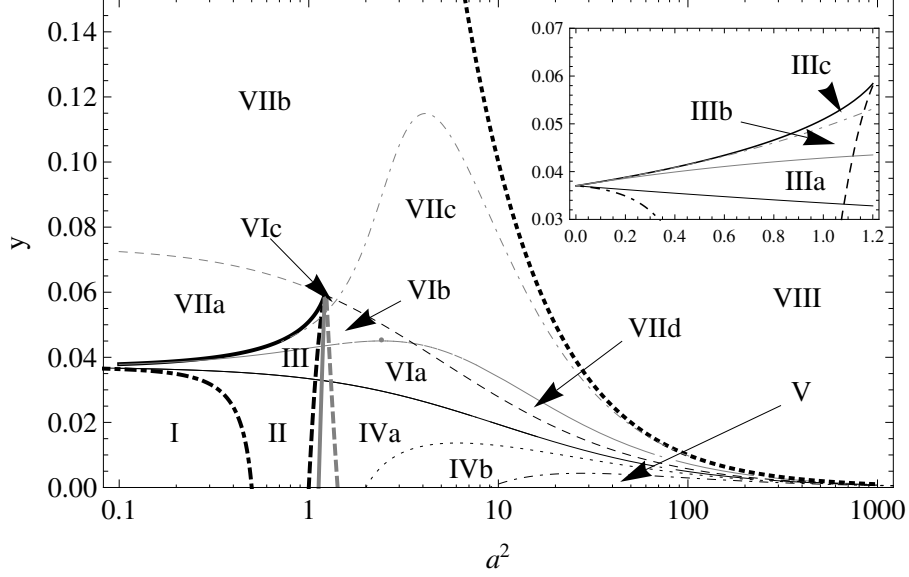


FIG. 7: The functions  $y_{max(h)}(a^2)$  (bold full black curve),  $y_{min(h)}(a^2)$  (bold dashed black curve),  $y_{d-z(ex)+}(a^2)$  (bold dash-dotted black curve),  $y_{max(d)}(a^2)$  (full black curve),  $y_{max(d(ex))}(a^2)$  (dashed grey/black curve),  $y_{ex(ex)-ex(ex)+}(a^2)$  (black dash-dotted),  $y_{d-ex(ex)+}(a^2)$  (dotted black curve),  $y_{ex(ex)-h}(a^2)$  (full grey curve),  $y_{ex(ex)-ex(ex)-}(a^2)$  (dash-dotted grey curve) and  $y = 1/a^2$  (bold dotted curve) giving division of parameter plane reflecting different character of the latitudinal motion. In order to clearly display the asymptotic behaviour of these functions we give their plots with the  $a^2$ -axis in logarithmic scale. All curves represent some qualitative changes in behaviour of characteristic functions  $q_r(r; y, a^2)$ ,  $q_{ex}(r; y, a^2)$ , which, however, are not all resulting in different character of photon motion. Such regions are then distinguished by different Roman numerals. Grey curves indicate some changes at negative - values of characteristic functions which are therefore irrelevant (see below for explanation). The bold grey lines are functions  $y_{(ex(ex)+)-(ex(ex)-)1}(a^2)$  (full) and  $y_{(ex(ex)+)-(ex(ex)-)2}(a^2)$  (dashed) needed for defining the function  $q_{min(ex\pm)}(y, a^2)$  in the following. The parts of these curves above their intersection, e. g. for  $y > y_{crit} = 0.0592$ , are irrelevant and therefore they are not depicted.

- the curve  $y_{max(d(ex))}(a^2)$  is given by functions  $a_{max(d(ex))}^2(r)$  and  $y_{d(ex)}(r; a^2 = a_{max(d(ex))}^2(r))$ ;

- $y_{d-z(ex)+}(a^2)$  is determined by

$$a_{d-z(ex)+}^2(r) \equiv \frac{r}{8}(1 - 4r + \sqrt{40r + 1})$$

and  $y_d(r; a^2 = a_{d-z(ex)+}^2(r))$ , where the function  $a_{d-z(ex)+}^2(r)$  is a solution of  $y_d(r; a^2) = y_{z(ex)+}(r; a^2)$  with respect to parameter  $a^2$ ; all such functions are obtained by analogous manner;

- $y_{ex(ex)-ex(ex)\pm}(a^2)$  are constructed from

$$a_{ex(ex)-ex(ex)\pm}^2(r) \equiv$$

$$\frac{r}{2}(4r^2 - 12r + 3 \pm \sqrt{16r^4 - 96r^3 + 156r^2 - 36r + 9})$$

and  $y_{ex(ex)}(r; a^2 = a_{ex(ex)-ex(ex)+}^2(r))$ ;

- $y_{d-ex(ex)+}(a^2)$  is given by  $a_{d-ex(ex)+}^2(r)$ , and e. g.  $y_d(r; a^2 = a_{d-ex(ex)+}^2(r))$ ; the analytical expression of the function  $a_{d-ex(ex)+}^2(r)$  is rather complex and therefore we shall not present it here;

- finally  $y_{ex(ex)-h}(a^2)$  we obtain from

$$a_{ex(ex)-h}^2(r) \equiv \frac{r}{2}(\sqrt{4r^2 - 12r + 1} - 1)$$

together with  $y_h(r; a^2 = a_{ex(ex)-h}^2(r))$ ;

There exist 15 regions in the  $a^2$ - $y$  plane corresponding to qualitatively different types of the behaviour of the characteristic functions  $q(r; y, a^2)$  that are in Fig. 7 visualized by full or dashed curves. The reason for using of these two styles of curves is that all the functions  $y(a^2)$  lie under the curve  $y = 1/a^2$ , and thus we have to take into account the restriction  $q \geq -a^2$  (see Section 1). Therefore, the changes of the characteristic functions  $q_r(r; y, a^2)$ ,  $q_{ex}(r; y, a^2)$  in values under this limit can be omitted as irrelevant. Moreover, we can easily show that in the case  $q < 0$ , the restrictions (53) imposed on the latitudinal motion yields stronger constraints on the value  $X$  than that given by the relations (59), (60), (61) conditioning the reality of the radial motion. Indeed, for any triad ( $q < 0, y, a^2$ ) there is no intersection of the curves  $X = X_{\pm}(r; q, y, a)$  with the lines  $X_{min(-)}^{\theta}$ ,  $X_{max(+)}^{\theta}$ , where  $X_{min(-)}^{\theta}$ ,  $X_{max(+)}^{\theta}$  are extrema of the functions  $X^{\theta}(m; q, y, a)$  introduced in Sec.1 (see Fig. 9 e-g,  $\omega$ ). To verify this, it is convenient to regard

the curves  $X = X_{\pm}(r; q, y, a)$  as  $q = \text{const.}$ -slices of a surface  $q = q_{\max}(r; X, a, y)$ , where

$$q \leq q_{\max}(r; X, a, y) \equiv \frac{(r^2 - aX)^2}{\Delta_r} - X^2 \quad (95)$$

is an alternative expression of the reality condition  $R(r; X, q, y, a) \geq 0$ , and search instead for intersections of surfaces  $q = q_{\max}(r; X, y, a)$  and  $q = q_{\min}(X, y, a)$ , defined by relations (54) - (58).

We therefore solve two equations -  $q_{\max}(r; X, y, a^2) = q_1(X)$ , with the result

$$X = \frac{r^2}{a}, \quad (96)$$

and  $q_{\max}(r; X, a, y) = q_2(X; a, y)$ , which gives

$$X_{1,2} = \frac{I^2 r^2 + 2(a^2 y - 1)\Delta_r \mp 2I\sqrt{-2r\Delta_r}}{a(I^2 - 4y\Delta_r)}. \quad (97)$$

The solution (96) yields  $X > 0$ , which, however, does not apply to the case  $q < 0$  for  $y < 1/a^2$ . Moreover, this solution represents touching points of the surface  $q_r(r; X, y, a^2)$  with the parabolic surface  $q_1(X)$  at  $X = +\sqrt{-q}$ , and hence can be omitted even in the case  $y \geq 1/a^2$ , since these values lie in the region forbidden by the relations (57)-(58). The solutions (97) are evidently irrelevant, since in stationary regions  $\Delta_r > 0$  they are imaginary.

The above analysis shows that in the case  $q < 0$  the 'potentials'  $X_{\pm}(r; q, y, a)$  have values in regions forbidden by reality conditions of the latitudinal motion and hence play no role at all. This is why there are in fact just seven regions in the  $(a^2-y)$ -plane relevant for different behaviour of the potentials  $X_{\pm}(r; q, y, a)$ , which are separated in Fig. 7 by solid lines. These areas are denoted by Roman numerals I-VII, the region No. VIII has to be introduced additionally in order to reflect different behaviour of the latitudinal motion.

The limits for impact parameter  $X$  of photons with  $q < 0$  are thus given by relation (53); photons satisfying the relation (53) have thus no turning points of the radial motion. In the rest of this treatise we can thus focus on the behaviour of the characteristic functions for  $q \geq 0$ . In Fig. 8 we present all possible variants of behaviour of the characteristic functions  $q(r; y, a^2)$ . These variants involve cases

**I:**  $y \leq y_{d-z(ex)+}(a^2)$  for  $a^2 \leq 0.5$

**II:**  $y_{d-z(ex)+}(a^2) \leq y \leq y_{\max(d)}(a^2)$  for  $a^2 \leq 0.5$ ,

or

$y \leq y_{\max(d)}(a^2)$  for  $0.5 \leq a^2 \leq 1$ ,

or

$y_{\min(h)}(a^2) \leq y \leq y_{\max(d)}(a^2)$  for  $1 \leq a^2 \leq 1.08316$ ;

**IIIa:**  $y_{\max(d)}(a^2) \leq y \leq y_{ex(ex)-h}(a^2)$  for  $a^2 \leq 1.08316$ ,

or

$y_{\min(h)}(a^2) \leq y \leq y_{ex(ex)-h}(a^2)$  for  $1.08316 \leq a^2 \leq 1.11949$ ;

**IIIb:**  $y_{ex(ex)-h}(a^2) \leq y \leq y_{ex(ex)-(ex(ex)-)}(a^2)$  for  $a^2 \leq 1.11949$ ,

or

$y_{\min(h)}(a^2) \leq y \leq y_{ex(ex)-(ex(ex)-)}(a^2)$  for  $1.11949 \leq a^2 \leq 1.16267$ ;

**IIIc:**  $y_{ex(ex)-(ex(ex)-)}(a^2) \leq y \leq y_{\max(h)}(a^2)$  for  $a^2 \leq 1.16267$ ,

or

$y_{\min(h)}(a^2) \leq y \leq y_{\max(h)}(a^2)$  for  $1.16267 \leq a^2 \leq 1.21202 = a_{crit}^2$ ;

**IVa:**  $y \leq y_{\min(h)}(a^2)$  for  $1 \leq a^2 \leq 1.08316$ ,

or

$y \leq y_{\max(d)}(a^2)$  for  $1.08316 \leq a^2 \leq 2$ ,

or

$y_{d-ex(ex)+}(a^2) \leq y \leq y_{\max(d)}(a^2)$  for  $a^2 \geq 2$ ;

**IVb:**  $y \leq y_{d-ex(ex)+}(a^2)$  for  $2 \leq a^2 \leq 9$ ,

or

$y_{ex(ex)-ex(ex)+}(a^2) \leq y \leq y_{d-ex(ex)+}(a^2)$  for  $a^2 \geq 9$ ;

**V:**  $y \leq y_{ex(ex)-ex(ex)+}(a^2)$  for  $a^2 \geq 9$

**VIa:**  $y_{\max(d)}(a^2) \leq y \leq y_{\min(h)}(a^2)$  for  $1.08316 \leq a^2 \leq 1.11949$ ,

or

$y_{\max(d)}(a^2) \leq y \leq y_{ex(ex)-h}(a^2)$  for  $1.11949 \leq a^2 \leq 3.56155$ ,

or

$y_{\max(d)}(a^2) \leq y \leq y_{\max(d(ex))}(a^2)$  for  $a^2 \leq 3.56155$ ;

**VIb:**  $y_{ex(ex)-h}(a^2) \leq y \leq y_{\min(h)}(a^2)$  for  $1.11949 \leq a^2 \leq 1.16267$ ,

or

$y_{ex(ex)-h}(a^2) \leq y \leq y_{ex(ex)-(ex(ex)-)}(a^2)$  for  $1.16267 \leq a^2 \leq 1.3983$ ,

or

$y_{ex(ex)-h}(a^2) \leq y \leq y_{\max(d(ex))}(a^2)$  for  $1.3983 \leq a^2 \leq 3.56155$ ;

**VIc:**  $y_{ex(ex)-(ex(ex)-)}(a^2) \leq y \leq y_{\min(h)}(a^2)$  for  $1.16267 \leq a^2 \leq 1.21202$ ,

or

$y_{ex(ex)-(ex(ex)-)}(a^2) \leq y \leq y_{\max(d(ex))}(a^2)$  for  $1.21202 \leq a^2 \leq 1.3983$ ;

**VIIa:**  $y_{\max(h)}(a^2) \leq y \leq y_{\max(d(ex))}(a^2)$  for  $a^2 \leq 1.21202$ ;

**VIIb:**  $y_{\max(d(ex))}(a^2) \leq y \leq 1/a^2$  for  $a^2 \leq 1.3983$ ,

or

$y_{ex(ex)-(ex(ex)-)}(a^2) \leq y \leq 1/a^2$  for  $a^2 \geq 1.3983$ ;

**VIIc:**  $y_{\max(d(ex))}(a^2) \leq y \leq y_{ex(ex)-(ex(ex)-)}(a^2)$  for  $1.3983 \leq a^2 \leq 3.56155$ ,

or

$y_{ex(ex)-h}(a^2) \leq y \leq y_{ex(ex)-(ex(ex)-)}(a^2)$  for  $a^2 \geq 3.56155$ ;



**VIIId:**  $y_{\max(d(ex))}(a^2) \leq y \leq y_{ex(ex)-h}(a^2)$  for  $a^2 \geq 3.56155$ ;

**VIII:**  $y \geq 1/a^2$ ;

The designation of the above introduced regions of the spacetime parameter  $a^2 - y$  space corresponds to the degree of importance of the curves in Figure 7 - curves dividing the parameter plane into regions of the same Roman numeral but with different letter of the Latin alphabet reflects some change in behaviour of the characteristic functions  $q(r; y, a^2)$  having no relevant impact on the behaviour of the potentials  $X_{\pm}(r; q, y, a^2)$ , the dashed curves relate with changes in negative values of the characteristic functions, which are therefore irrelevant (cf. e. g. Figs. 8c-8e).

Now it remains to assign to each region in the  $(a^2 - y)$ -plane functions  $q(y, a^2)$ , which by themselves represent marginal values of the parameter  $q$  corresponding to some qualitative shift in the behaviour of the potentials  $X_{\pm}(r; q, y, a^2)$ .

In the regions I, II which describe black hole spacetimes with divergent repulsive barrier, we have to compare the two local maxima  $q_{\max(ex+)}(y, a^2)$  located under the inner horizon and  $q_{\max(ex)}(y, a^2) = q_{\min(r)}(y, a^2)$  between the outer and cosmological horizons respectively (see Figs. 8a,b). The function  $q_{\max(ex+)}(y, a^2)$  is given parametrically by functions  $y_{ex(ex)+}(r; y, a^2)$  and  $q_{ex}(r; y = y_{ex(ex)+}(r; y, a^2), a^2)$  with  $r$  being the parameter, similarly  $q_{\max(ex)}(y, a^2)$  is given by  $y_{ex(ex)}(r; y, a^2)$  and  $q_{ex}(r; y = y_{ex(ex)}(r; y, a^2), a^2)$ .

The extrema function  $q_{\max(ex)}(y, a^2)$  diverges at the curve  $y_{\max(d)}(a^2)$ , which forms boundary between regions II-III and IV-VI, i. e.  $q_{\max(ex)}(y = y_{\max(d)}(a^2), a^2) \rightarrow +\infty$  (c. f. Figs. 8b, 8c and 8f, 8i). In the region III, corresponding to black hole spacetimes with the restricted repulsive barrier, only local maximum  $q_{\max(ex+)}(y, a^2)$  located under the inner horizon remains. As can be seen from the behaviour of the characteristic functions in Fig. 6b, for  $y \rightarrow y_{\min(h)}(a^2)$  from above, the 'inner' local maximum of  $q_{(ex)}(r; y, a^2)$ , determined by  $y_{ex(ex)+}(r; y, a^2)$ , approaches from the left its divergency point given by  $y = y_{d(ex)}(r; a^2)$ , where  $q_{ex} \rightarrow -\infty$  (Fig. 8b), so that  $q_{ex}(r; y = y_{\min(h)}(a^2), a^2)$  becomes continuous. For  $y \leq y_{\min(h)}(a^2)$ , the divergency of the function  $q_{ex}(r; y, a^2)$  appears again with  $q_{ex} \rightarrow +\infty$  and a local minimum has formed on the right (cf. Figs. 8b, 8f). Hence the curve  $y_{\min(h)}(a^2)$  forms a boundary on which the local maxima  $q_{\max(ex+)}(y, a^2)$  convert into local minima. We denote them  $q_{\min(ex\pm)}(y, a^2)$ , since, as follows from relations (86)-(91), for  $1.125 \leq a^2 \leq a_{crit}^2$  and

$$y \leq y_{(ex(ex)+)-(ex(ex)-)1}(a^2) \equiv \frac{8a^2 - 9}{8a^4} \quad (98)$$

or  $a_{crit}^2 \leq a^2 \leq 1.3923$  and

$$y \leq y_{(ex(ex)+)-(ex(ex)-)2}(a^2) \equiv \sqrt{\frac{3(2\sqrt{3}-3)}{a^6}} - \frac{1}{a^2} \quad (99)$$

they are given by  $y_{ex(ex)-}(r; y, a^2)$ . The function  $y_{(ex(ex)+)-(ex(ex)-)1}(a^2)$  is given parametrically by  $a_{r(ex(ex)\pm)}^2(r)$  and, e. g., by  $y_{ex(ex)-}(r; y, a^2 = a_{r(ex(ex)\pm)}^2(r))$ , and the function  $y_{(ex(ex)+)-(ex(ex)-)2}(a^2)$  by  $a_{r(ex(ex)\pm)+}^2(r)$  and  $y_{ex(ex)-}(r; y, a^2 = a_{r(ex(ex)\pm)+}^2(r))$ . The analytical expressions in (98), (99) can be then derived by eliminating the radius  $r$ . Both these functions have their relevant parts entirely in regions IV, VI (see Fig. 7).

We have to relate the minima  $q_{\min(ex\pm)}(y, a^2)$  with the maxima  $q_{\max(ex)}(y, a^2) = q_{\min(r)}(y, a^2)$ . In the region V, the minima of  $q_{ex}(r; y, a^2)$  coalesce with the minima of  $q_r(r; y, a^2)$  (Fig. 8h). We therefore have to compare the function  $q_{\min(ex)}(y, a^2) = q_{\min(r)}(y, a^2)$  determined by  $y_{ex(ex)}(r; y, a^2)$  and, e. g.,  $q_{ex}(r; y = y_{ex(ex)}(r; y, a^2), a^2)$ , with local maxima  $q_{\max(ex+)}(y, a^2)$  parametrized by  $y_{ex(ex)+}(r; y, a^2)$  and  $q_{ex}(r; y = y_{ex(ex)+}(r; y, a^2), a^2)$ . The boundary curve  $y_{ex(ex)-ex(ex)+}(a^2)$  then represents such combinations of parameters  $a^2, y$  for which the local extrema of  $q_{ex}(r; y, a^2)$  have coalesced into an inflection point. For parameters from the region VI, corresponding to naked singularity spacetimes with restricted repulsive barrier (as well as from the remaining regions VII, VIII), the function  $q_{ex}(r; y, a^2)$  has one local minimum (Figs. 8i, j, k) and we therefore construct a function  $q_{\min(ex\pm)}(y, a^2)$  determined by functions  $y_{ex(ex)\pm}(r; a^2)$  and  $q_{ex}(r; y = y_{ex(ex)\pm}(r; a^2), a^2)$ , where the minus sign has to be chosen for  $1.17007 \leq a^2 \leq a_{crit}^2$  and  $y_{\max(d)}(a^2) \leq y \leq y_{(ex(ex)+)-(ex(ex)-)1}(a^2)$ , or  $a_{crit}^2 \leq a^2 \leq 1.2828$  and  $y_{\max(d)}(a^2) \leq y \leq y_{(ex(ex)+)-(ex(ex)-)2}(a^2)$  (see Fig. 7). For  $y \rightarrow y_{\max(d(ex))}(a^2)$  and  $a^2 \geq a_{crit}^2$  there is  $q_{\min(ex+)}(y, a^2) \rightarrow +\infty$ , and for  $y > y_{\max(d(ex))}(a^2)$ , i. e. in the region VII, it converts into the local maximum (c.f., e. g., Figs 8j, 8n). The transition into the region VII from the region III can be inferred from comparison of Fig. 8c with Fig. 8l. Therefore, in the region VII we have to follow up the values of the function  $q_{\max(ex+)}(y, a^2)$  determined by the functions  $y_{ex(ex)+}(r; a^2)$  and  $q_{ex}(r; y = y_{ex(ex)+}(r; a^2), a^2)$ . The dashed curves in Fig. 7 indicate some changes at negative values of the characteristic functions  $q(r; y, a^2)$  (c. f. e. g. Figs 8l, 8m) which are therefore irrelevant. The functions  $q(y, a^2)$  are demonstrated in Fig. 9.

With the knowledge of the behaviour of the extremal values  $q_{\min/\max(ex)}(y, a^2)$  at each region in the  $(a^2 - y)$ -plane we finally constructed all qualitatively different types of the effective potentials  $X_{\pm}(r; q, y, a)$ . They are presented in Figure 10 for appropriately chosen representative combinations  $(q, y, a^2)$ .

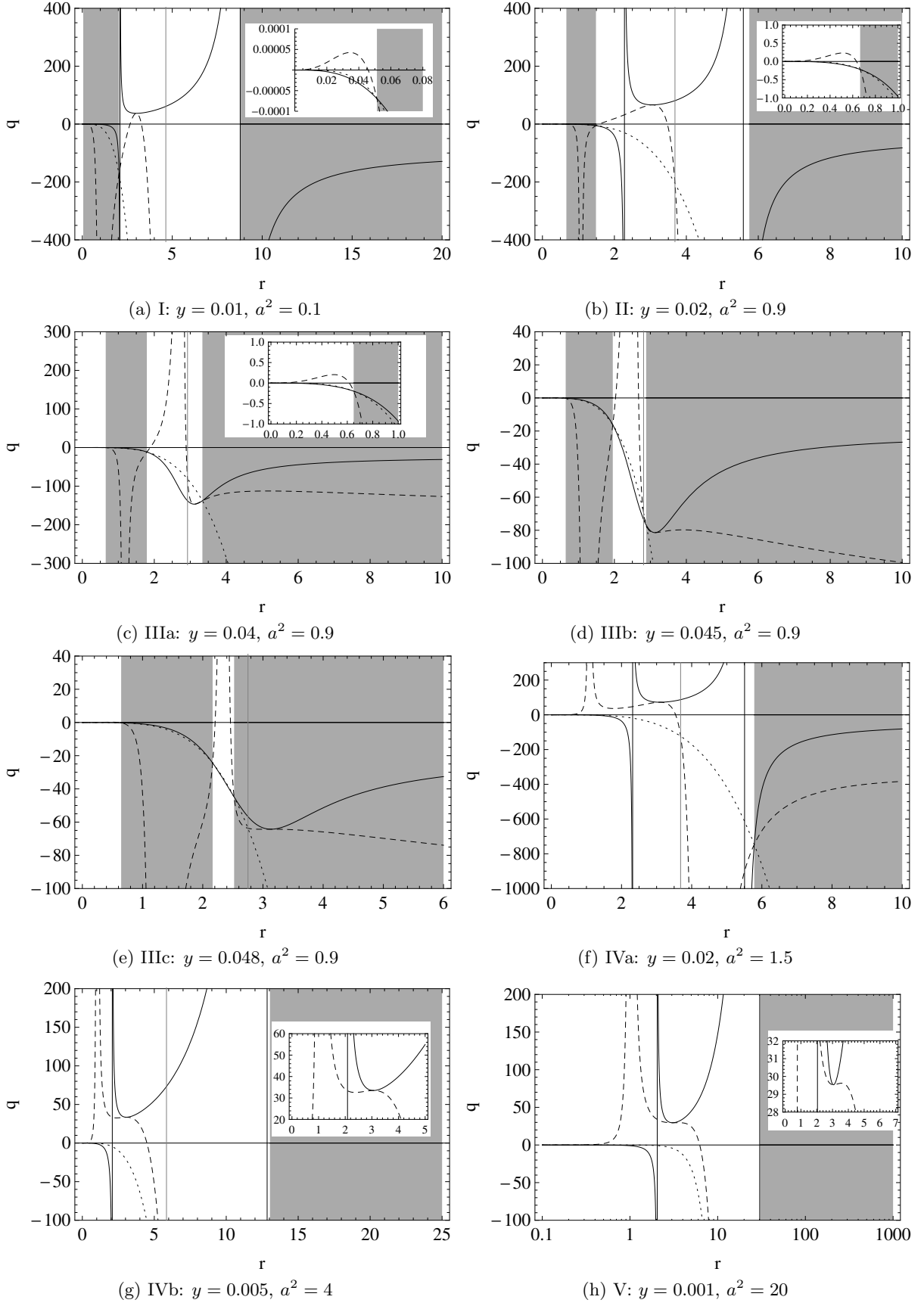


(Figure continued)

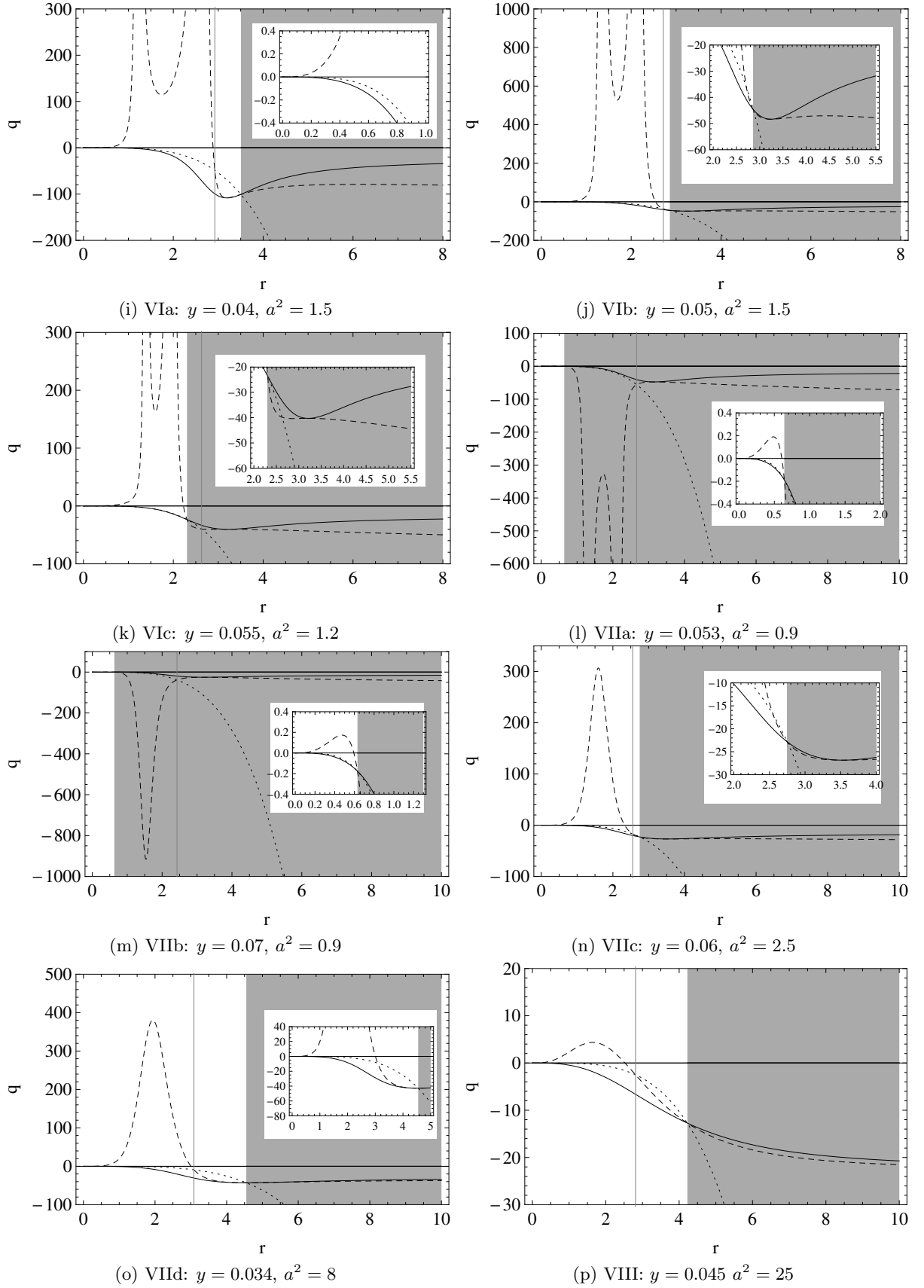


FIG. 8: Characteristic functions  $q_r(r; y, a^2)$  (full curve),  $q_{ex}(r; y, a^2)$  (dashed curve) and  $q_{ex1}(r; y, a^2)$  (dotted curve) governing the behaviour of effective potentials  $X_{\pm}(r; q, y, a)$ . The dynamic region is highlighted by shading, the grey vertical bar demarcates loci of the static radius. Note that the last scheme corresponding to case  $y > 1/a^2$ , which is introduced due to changes in the latitudinal motion, brings no new features in character of the radial motion, since it qualitatively coincide with case VIIb and is shown for completeness.

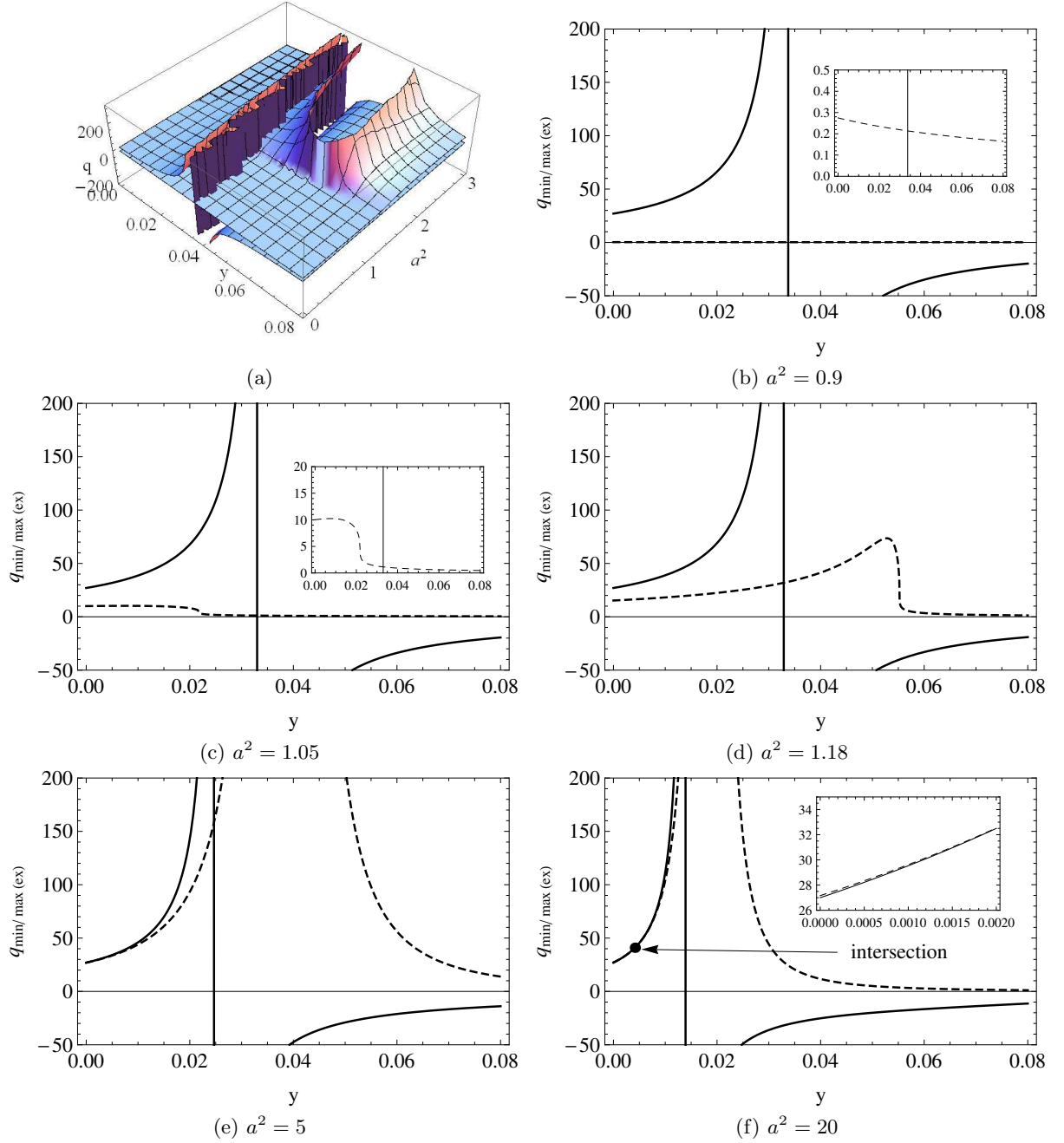
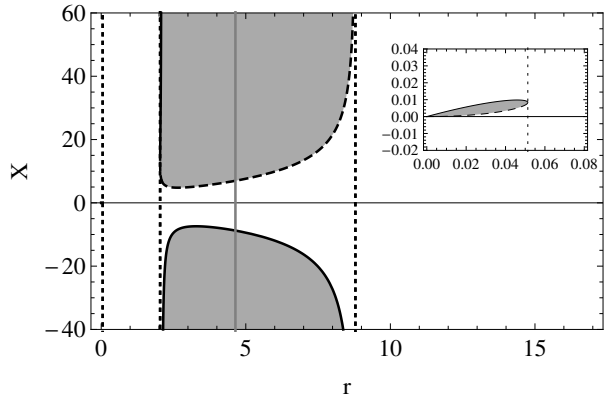
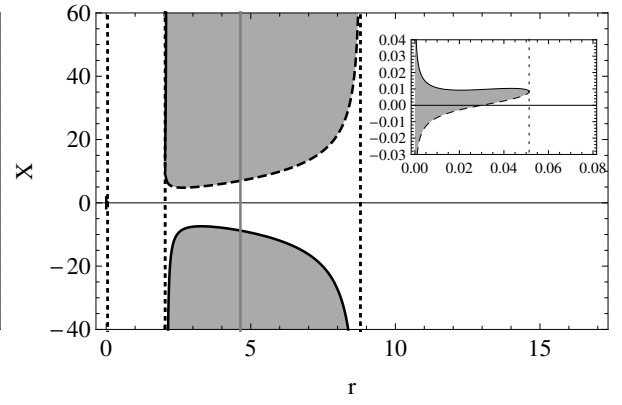
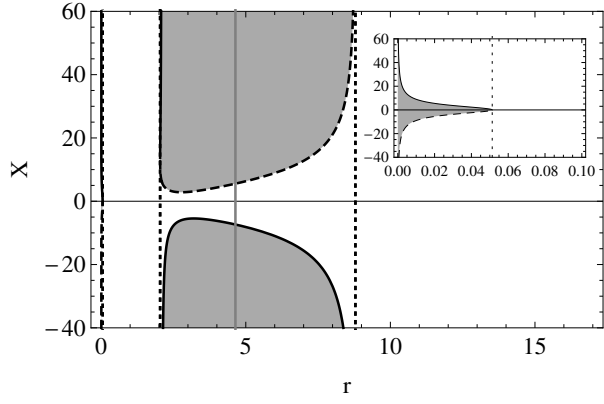
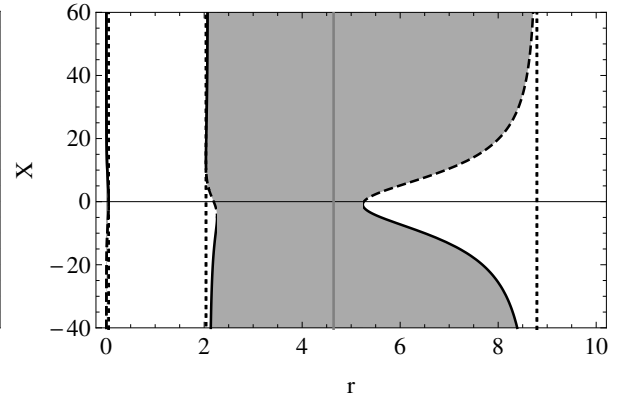
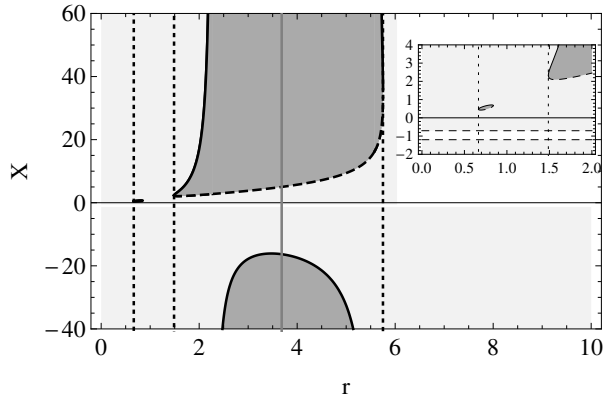
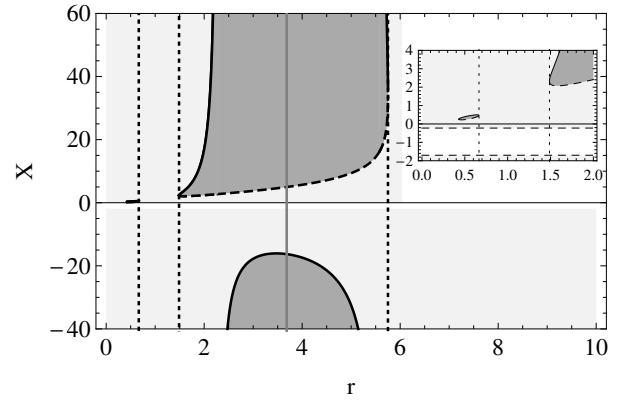
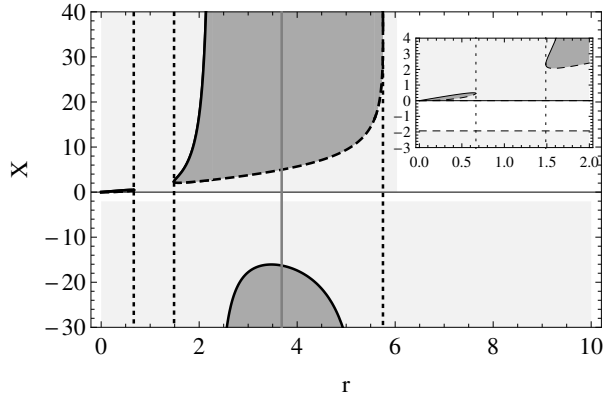
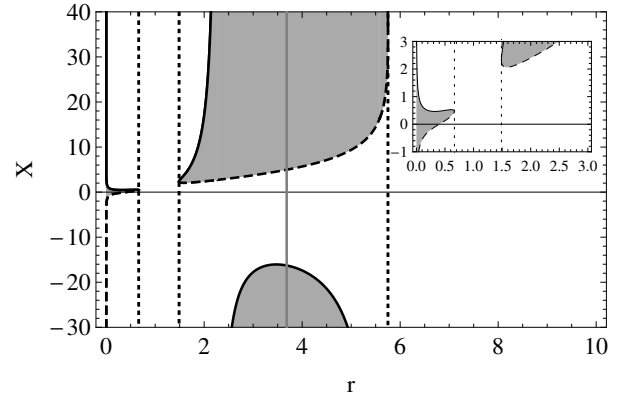
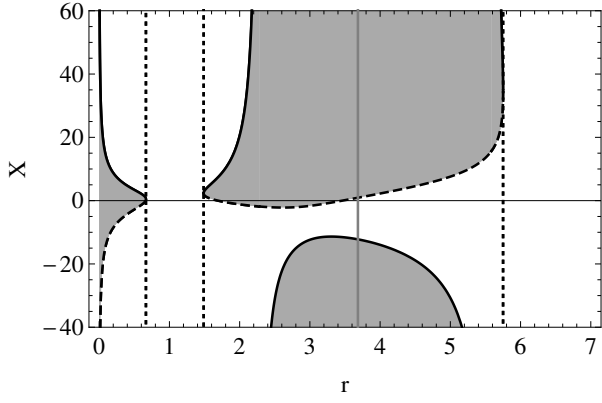
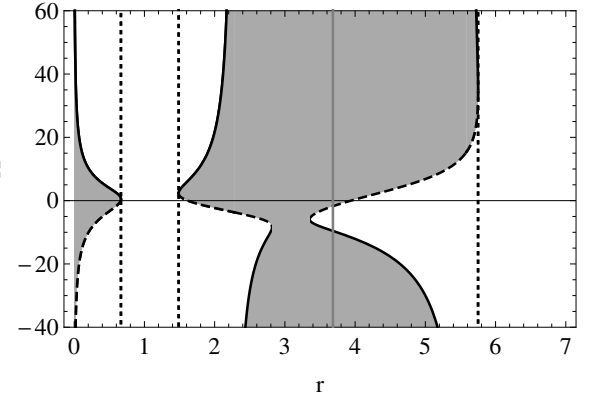
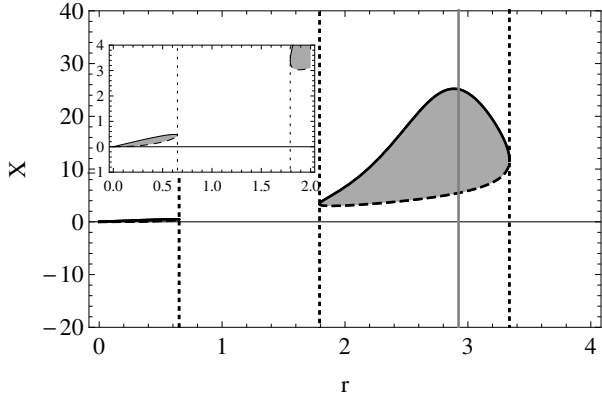
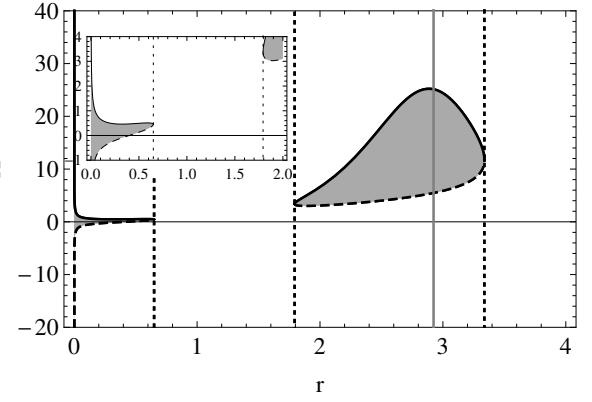
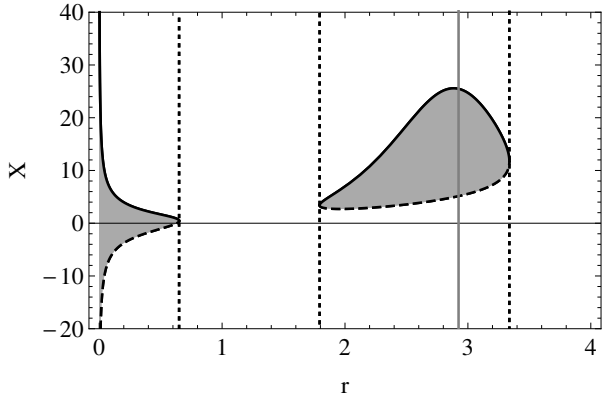
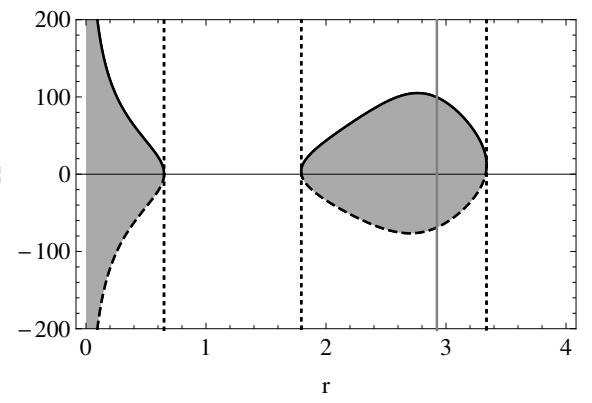
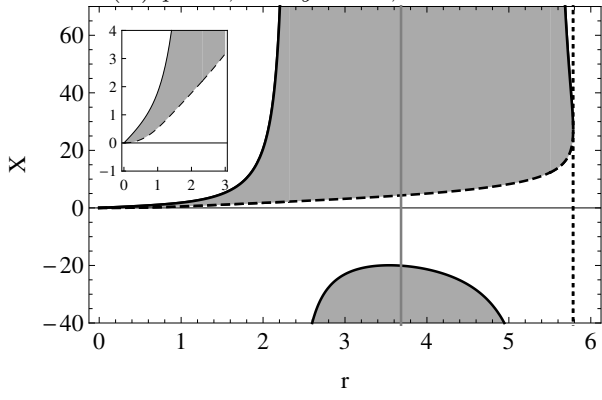
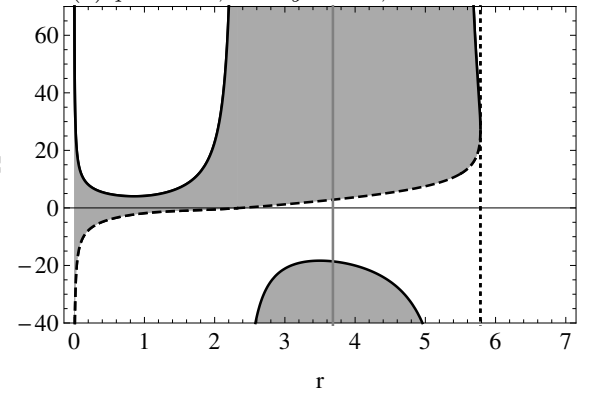
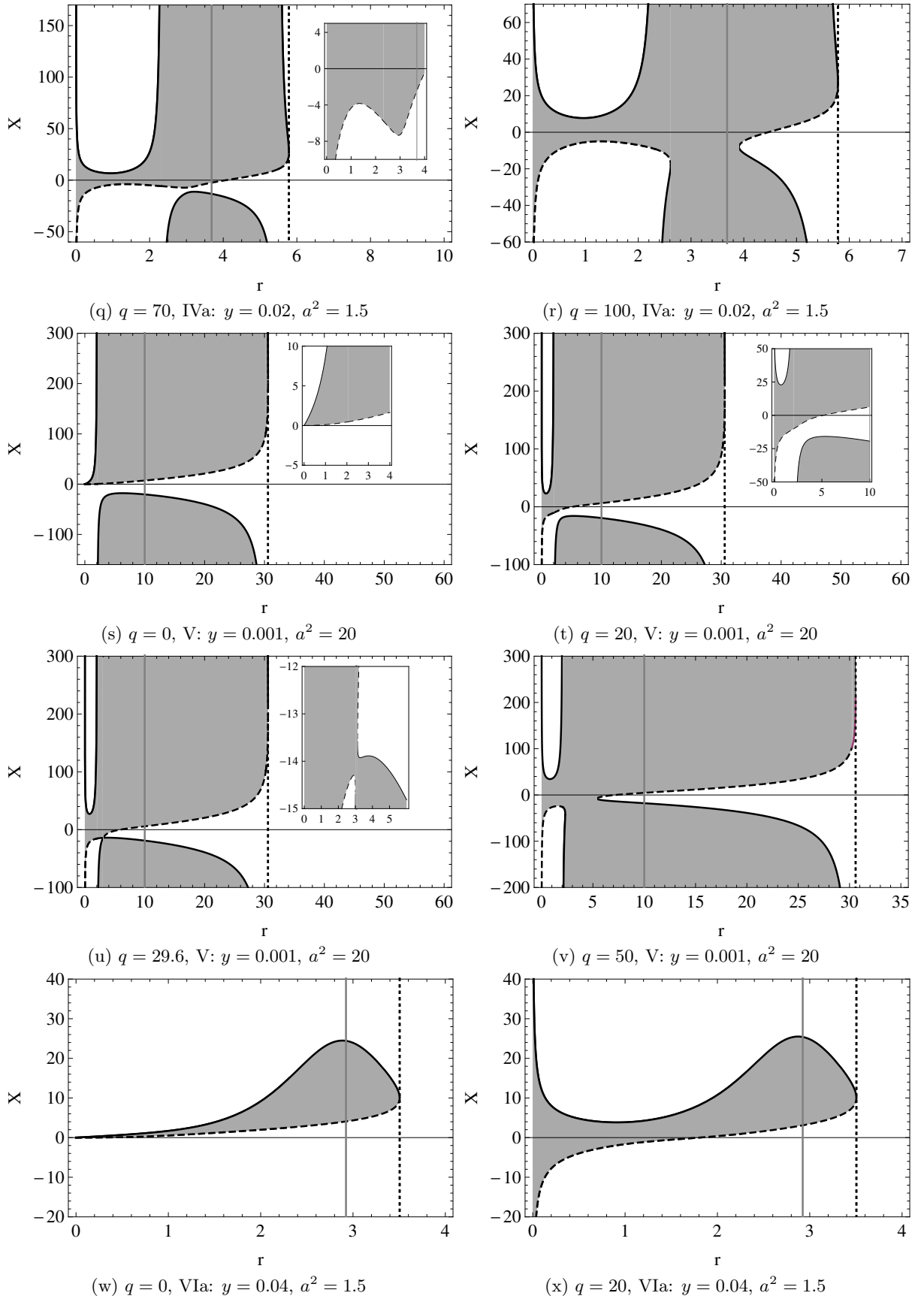


FIG. 9: 3D plot of functions  $q(y, a^2)$  (a) and its  $a^2 = \text{const.}$ -slices corresponding to values between outstanding limits  $a^2 = 1, a_{rrb(max)}^2 = 1.08316, a_{crit}^2 = 1.21202$  and  $a_{(ex(ex)-ex(ex)+)min}^2 = 9$ . The positive branch of the full curve is the graph of the function  $q_{max(ex)}(y, a^2)$ , its asymptote intersects the  $(a^2-y)$ -plane in the curve  $y_{max(d)}(a^2)$ . The dashed curve in Fig. (b) describes the local maxima  $q_{max(ex+)}(y, a^2)$  under the inner horizon. In Figs. (c), (d) it represents local minima  $q_{min(ex+)}(y, a^2)$  ( $q_{min(ex-)}(y, a^2)$  eventually) for  $y < y_{min(h)}(a^2)$ , and maxima  $q_{max(ex+)}(y, a^2)$  for  $y > y_{min(h)}(a^2)$ , where the critical value  $q_{max(ex+)}(y = y_{min(h)}(a^2), a^2)$  can be identified as the inflection point of this curve. The minima diverge as  $y \rightarrow y_{max(d(ex))}(a^2)$  (Fig. e), the descending part then describes the local maxima  $q_{max(ex+)}(y, a^2)$  in region VII. Fig. (f) demonstrates intersection of both curves at  $y = y_{ex(ex)-ex(ex+)}(a^2)$ . The full curve for  $y < y_{ex(ex)-ex(ex+)}(a^2)$  then corresponds to the local minima  $q_{min(ex)}(y, a^2) = q_{min(r)}(y, a^2)$ , while the dashed one now matches the maxima  $q_{max(ex+)}(y, a^2)$ .

(a)  $q = 0$ , I:  $y = 0.01$ ,  $a^2 = 0.1$ (b)  $q = 2.10^{-5}$ , I:  $y = 0.01$ ,  $a^2 = 0.1$ (c)  $q = 20$ , I:  $y = 0.01$ ,  $a^2 = 0.1$ (d)  $q = 80$ , I:  $y = 0.01$ ,  $a^2 = 0.1$ (e)  $q = -0.5$ , II:  $y = 0.02$ ,  $a^2 = 0.9$ (f)  $q = -0.05$ , II:  $y = 0.02$ ,  $a^2 = 0.9$ (g)  $q \rightarrow 0^-$ , II:  $y = 0.02$ ,  $a^2 = 0.9$ (h)  $q = 0.1$ , II:  $y = 0.02$ ,  $a^2 = 0.9$ 

(Figure continued)

(i)  $q = 50$ , II:  $y = 0.02$ ,  $a^2 = 0.9$ (j)  $q = 70$ , II:  $y = 0.02$ ,  $a^2 = 0.9$ (k)  $q = 0$ , IIIa:  $y = 0.04$ ,  $a^2 = 0.9$ (l)  $q = 0.1$ , IIIa:  $y = 0.04$ ,  $a^2 = 0.9$ (m)  $q = 10$ , IIIa:  $y = 0.04$ ,  $a^2 = 0.9$ (n)  $q = 10000$ , IIIa:  $y = 0.04$ ,  $a^2 = 0.9$ (o)  $q = 0$ , IVa:  $y = 0.02$ ,  $a^2 = 1.5$ (p)  $q = 20$ , IVa:  $y = 0.02$ ,  $a^2 = 1.5$



(Figure continued)

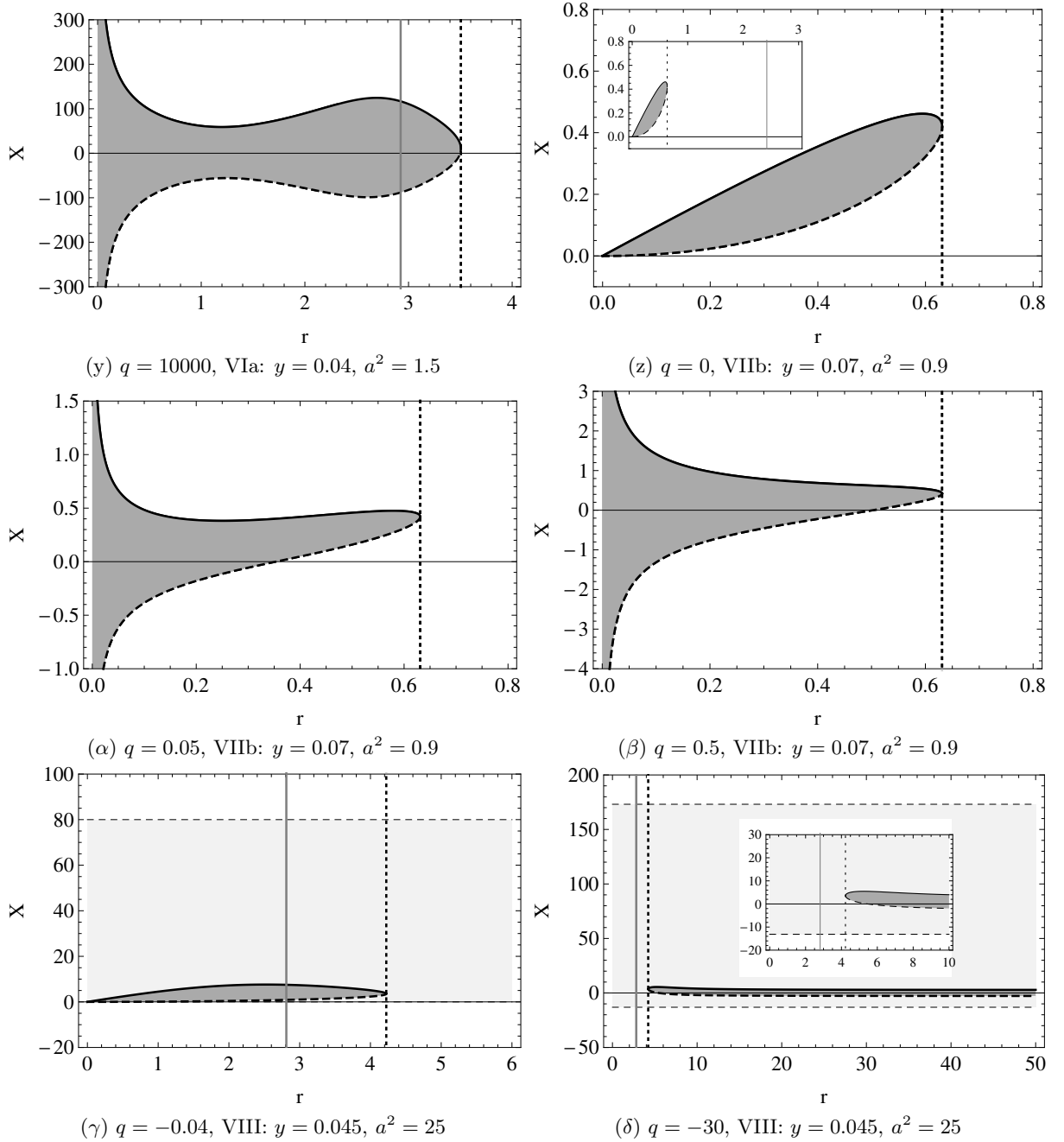


FIG. 10: Different types of behaviour of the potentials  $X_+(r; q, a, y)$  (full curve), and  $X_-(r; q, a, y)$  (dashed curve), with spacetime parameters chosen successively from regions corresponding to the classes I-VIII in the  $(a^2 - y)$ -plane, and some representative values of parameter  $q$  divided by the extrema  $q(y, a^2)$ . Vertical dashed lines demarcate loci of the event horizons, the grey line demarcate the static radius, shading highlights the forbidden region. Figs. (e)-(g) depict the case  $q < 0$  with the limiting values  $X_{min(-)}$ ,  $X_{max(+)}$  as horizontal dashed lines. The graphs  $X_{\pm}(r; q, a, y)$  lie entirely in forbidden region. The behaviour of these functions in other cases differing by values  $a, y$  with  $q < 0$  is qualitatively the same. Figs. (γ)-(δ) describes the case  $y > 1/a^2$ ,  $q < 0$ . The potentials have values in forbidden region again.

## V. CLASSIFICATION OF THE KERR-DE SITTER SPACETIMES ACCORDING TO PROPERTIES OF THE PHOTON MOTION

In the following section we demonstrate by using the behaviour of the effective potentials  $X_{\pm}(r; q, a, y)$  that

the null geodesics create qualitatively different structures in the individual cases of Kerr-de Sitter spacetimes with spacetime parameters chosen from different parts in the  $(a^2 - y)$ -plane labelled by numerals I-VIII and hence that regions of the parameter space of these labels can be considered as classification of Kerr-de Sitter spacetimes due



to the photon motion. Similarly as in [66], the main criterion for this classification is the number of the event horizons. Another differentiating factors follow from the nature of photon motion. There is some kind of repulsive barrier defending a light to reach the ring singularity, which is always created in its vicinity for photons with  $q > 0$ . However, a similar barrier can emerge between the outer black hole horizon and the cosmological horizon in black hole spacetimes repelling photons towards one of these horizons. In the naked singularity spacetimes, occurrence of such an additional barrier, which reflects photons towards the ring singularity or cosmological horizon, leads to the phenomenon of bound photon orbits. Such orbits are not present in the case of the black hole spacetimes. The presence and character of this barrier we take as another criterion in the following classification. The third aspect that authorizes us to make such distinction will be the existence and character of spherical photon orbits.

We characterize the properties of the photon motion in these eight classes of the Kerr-de Sitter spacetimes in the following way:

**Class I :** Black hole spacetimes with the divergent repulsive barrier of the radial photon motion, having one equatorial circular orbit located under the inner black hole horizon ( $r = r_-$ ) and two equatorial circular orbits located at  $r = r_{ph+}$ ,  $r = r_{ph-}$ ,  $r_{ph+} < r_{ph-}$ , between the outer black hole ( $r = r_+$ ) and the cosmological ( $r = r_c$ ) horizon for  $q = 0$ , all being unstable relative to radial perturbations (Fig. 10(a)). The photons at radii  $r = r_{ph+}$  ( $r = r_{ph-}$ ) are co-rotating (counter-rotating) relative to the family of locally non-rotating observers [8]. Two spherical photon orbits occur under the inner black hole horizon for  $0 < q < q_{max(ex+)}(y, a^2)$ , the inner one being stable, the outer one being unstable (Fig. 10(b)). These orbits coalesce for  $q = q_{max(ex+)}(y, a^2)$  (c. f. details in Figs. 10(b, c)). Between the outer black hole and the cosmological horizon there exist two unstable spherical photon orbits between  $r_{ph+}$ ,  $r_{ph-}$  for  $0 < q < q_{max(ex)}(y, a^2)$ , being confined to the regions where  $\Delta_r > a^2$ , i. e., between the radii given by (67). If we denote them  $r_{d1}$ ,  $r_{d2}$ , then it holds  $r_+ < r_{d1} < r_{ph+} < r_{ph-} < r_{d2} < r_c$ . These orbits merge for  $q = q_{max(ex)}(y, a^2)$  and for  $q > q_{max(ex)}(y, a^2)$  a barrier of radial photon motion is formed between the outer and cosmological horizon for any impact parameter  $X$  (Fig. 10(d)).

**Class II :** Black hole spacetimes with the same features as in the class I, but now there is  $r_+ < r_{ph+} < r_{d1} < r_{ph-} < r_{d2} < r_c$ , i. e., the inner circular equatorial orbit and some spherical orbits with  $X = X_{min(-)}(r)$ , and parameter  $q$  small enough enter regions where  $0 < \Delta_r < a^2$  (Fig. 10(h)); here we denoted by  $X_{min(-)}(r)$  the local minimum of the potential  $X_-(r; q, y, a)$ , in order to avoid confusion

with the limits imposed by the reality conditions of the latitudinal motion.

**Class III :** Black hole spacetimes with the restricted repulsive barrier of the radial photon motion. The same conclusions hold for the radial photon motion under the inner black hole horizon (Figs. 10(k)-(m)), as in classes I, II, but between the outer black hole and the cosmological horizon the photons can move freely for any  $X < X_{min(-)}(r)$  or  $X > X_{max(+)}(r)$ , where the limits correspond to unstable spherical orbits. For  $q$  increasing, the limits diverge, i. e., there is  $X_{min(-)}(r) \rightarrow -\infty$ ,  $X_{max(+)}(r) \rightarrow +\infty$  as  $q \rightarrow +\infty$  (Fig. 10(n)).

**Class IV :** Naked singularity spacetimes with the divergent repulsive barrier of the radial photon motion. The ring singularity can be reached by photons with  $q = 0$  and  $X_{max(+)}(r) < X \leq 0$ , case  $X = X_{max(+)}(r)$  corresponds to the unstable circular equatorial photon orbit (Fig. 10(o)). Two spherical orbits exist for  $0 < q < q_{min(ex+)}(y, a^2)$  ( $q_{min(ex-)}(y, a^2)$  respectively), the inner one stable, the outer unstable (Fig. 10(p)). If,  $q_{min(ex\pm)}(y, a^2) < q < q_{max(ex)}(y, a^2) = q_{min(r)}(y, a^2)$ , then two other spherical orbits occur, those internal two are then stable, the two outer ones being unstable (Fig. 10(q)). For  $q > q_{max(ex)}(y, a^2)$ , the unstable orbits have coalesced and a barrier is formed for any parameter  $X$  between the ring singularity and the cosmological horizon (Fig. 10(r)).

**Class V :** Naked singularity spacetimes with the same features of the photon motion as in class IV, for  $q$  small enough, but now two spherical orbits - the inner one stable, the outer unstable - exist for  $0 < q < q_{min(ex)}(y, a^2) = q_{min(r)}(y, a^2)$  (Fig. 10(t)). For  $q_{min(ex)}(y, a^2) < q < q_{max(ex+)}(y, a^2)$  a barrier for any  $X$  arises, while the unstable photon spherical orbit splits into three spherical orbits, the most outer one being the only unstable (Fig. 10(u)), which coalesce again with the neighbouring stable spherical orbit after a small increase to  $q > q_{max(ex+)}(y, a^2)$  (Fig. 10(v)).

**Class VI :** Naked singularity spacetimes with the restricted repulsive barrier of the radial photon motion. For  $q = 0$ , there is one unstable equatorial circular photon orbit (Fig. 10(w)), for  $0 < q < q_{min(ex+)}(y, a^2)$ , there exist two spherical orbits - the inner one stable, the outer one unstable (Fig. 10(x)), photons with  $q > q_{min(ex+)}(y, a^2)$  can occupy four spherical orbits - two inner ones being stable, the outer ones, enclosing the height of this barrier, being unstable (Fig. 10(y)).

**Class VII :** Naked singularity spacetimes with the restricted repulsive barrier of the radial photon motion having one unstable equatorial circular photon

orbit with  $q = 0$  (Fig. 10(z), two spherical orbits for  $0 < q < q_{max(ex+)}(y, a^2)$ , the inner one being stable, the outer one - unstable - located close to the cosmological horizon (Fig. 10( $\alpha$ )), while no spherical orbits exist for  $q > q_{max(ex+)}(y, a^2)$  (Fig. 10( $\beta$ )).

**Class VIII :** Special class of the naked singularity spacetimes demonstrating the same features of the radial motion of photons with  $q \geq 0$  as in the class VII, but differing from all previous cases by the existence of null geodesics for arbitrary  $q < 0$ . The allowed values of the impact parameter  $X$  are confined to the intervals  $X < X_{max(+)}^\theta < 0$  or  $X > X_{min(-)}^\theta > 0$  (see Section 3). The potentials governing the radial photon motion are fully immersed in the forbidden region (Figs. 10( $\gamma$ ), ( $\delta$ )), thus in the radial direction the photons with such parameters move freely in the whole range between the ring singularity and the cosmological horizon.

## VI. CONCLUSIONS

We can summarize our results by the following concluding remarks.

1. In any kind of the black hole spacetimes, there are no radially bound null geodesics in the stationary region, i. e., the trajectory of a photon has at most one turning point in radial direction between the outer and cosmological horizon, or the photons can move freely between the outer black hole and the cosmological horizons. However, such bounded photon orbits exist in each naked singularity spacetime for photons with parameters  $q > 0$  and  $X$  chosen appropriately.
2. No photons with  $q > 0$  can reach the ring singularity at  $r = 0$  in any of the Kerr-de Sitter spacetimes.
3. In the Kerr-de Sitter spacetimes of classes I-VII, i. e., with spacetime parameters satisfying the condition  $y < 1/a^2$ , there is a lower limit  $q = -a^2$  of the parameter  $q < 0$ , for which the photon motion is allowed. The range of the allowed values of the impact parameter  $X$  is then an interval given by the relations (53) - (56). Photons with such tuned parameters have no turning point in radial direction, since the effective potential lies entirely in the forbidden region (Figs.10(e), 10(f)). Further, by the results of Section 3, only such photons execute the vortical motion, or their trajectory lies completely on the cones of  $\theta = \text{constant}$ . We can therefore reject possibility of existence of vortical photon motion of constant radius, or off-equatorial circular photon orbits.
4. In the Kerr-de Sitter spacetimes of class VIII ( $y > 1/a^2$ ), the photon motion is allowed for any  $q < 0$ . The permissible values of the parameter  $X$  are then two disjunct unlimited intervals determined by the relation (58.) In the extreme case  $y = 1/a^2$ , it must be  $q \geq -a^2$  again and for negative  $q$ , the parameter  $X$  can take less than certain negative value given by (57). The consequences for photon motion are then the same as in previous note (Figs. 10( $\gamma$ )-( $\delta$ )).
5. In the Kerr-de Sitter spacetimes with the divergent repulsive barrier of the radial photon motion, there exists a critical value  $q_{max(ex)}(y, a^2)$ , for which this barrier becomes impermeable between the outer black hole horizon and cosmological horizon, or, in naked singularity spacetimes, between the ring singularity and cosmological horizon, for photons with any impact parameter  $X$ . In spacetimes with the restricted repulsive barrier of the radial photon motion, the height of this barrier slowly grows with increasing parameter  $q$ , but stays finite for any  $q > 0$  (Figs. 10(n), 10(y)).

- 
- [1] C. Adami, F. Durret, L. Guennou, and C. Da Rocha. Diffruse light in the young cluster of galaxies CL J1449+0856 at  $z = 2.07$ . *Astronomy and Astrophysics*, 551:A20 (7 pages), Mar. 2013.
  - [2] A. N. Aliev. Electromagnetic properties of Kerr-anti-de Sitter black holes. *Phys. Rev. D*, 75(8):084041, Apr. 2007.
  - [3] C. Armendariz-Picon, V. Mukhanov, and P. J. Steinhardt. Dynamical solution to the problem of a small cosmological constant and late-time cosmic acceleration. *Phys. Rev. Lett.*, 85(21):4438, 2000.
  - [4] I. Arraut. Komar mass function in the de Rham-Gabadadze-Tolley nonlinear theory of massive gravity. *Phys. Rev. D*, 90:124082, Dec 2014.
  - [5] B. Aschenbach. Measurement of Mass and Spin of Black Holes with QPOs. *Chinese Journal of Astronomy and Astrophysics Supplement*, 8:291-296, Oct. 2008.
  - [6] N. Bahcall, J. P. Ostriker, S. Perlmutter, and P. J. Steinhardt. The cosmic triangle: Revealing the state of the universe. *Science*, 284:1481-1488, 1999.
  - [7] P. Bakala, P. Čermák, S. Hledík, Z. Stuchlík, and K. Truparová. Extreme gravitational lensing in vicinity of Schwarzschild-de Sitter black holes. *Central European J. Phys.*, 5(4):599-610, Dec. 2007.
  - [8] J. M. Bardeen. Timelike and null geodesics in the Kerr metric. In C. Dewitt and B. S. Dewitt, editors, *Black Holes (Les Astres Occlus)*, pages 215-239, 1973.
  - [9] J. Bičák and Z. Stuchlík. On the latitudinal and radial motion in the field of a rotating black hole. *Bull. Astronom. Inst. Czechoslovakia*, 27(3):129-133, 1976.
  - [10] C. G. Böhmer. Eleven Spherically Symmetric Constant Density Solutions with Cosmological Constant. *Gen. Rel-*

- activity *Gravitation*, 36:1039–1054, May 2004.
- [11] E. K. Boyda, S. Ganguli, P. Hořava, and U. Varadarajan. Holographic Protection of Chronology in Universes of the Gödel Type. *Phys. Rev. D*, 67:106003, 2003.
  - [12] R. Caldwell and M. Kamionkowski. Cosmology: Dark matter and dark energy. *Nature*, 458(7238):587–589, Apr. 2009.
  - [13] R. R. Caldwell, R. Dave, and P. J. Steinhardt. Cosmological imprint of an energy component with general equation of state. *Phys. Rev. Lett.*, 80(8):1582, 1998.
  - [14] B. Carter. Black hole equilibrium states. In C. Dewitt and B. S. Dewitt, editors, *Black Holes (Les Astres Occlus)*, pages 57–214, 1973.
  - [15] J.-H. Chen and Y.-J. Wang. Influence of dark energy on time-like geodesic motion in Schwarzschild spacetime. *Chinese Physics B*, 17(4):1184, 2008.
  - [16] N. Cruz, M. Olivares, and J. R. Villanueva. The geodesic structure of the Schwarzschild anti-de Sitter black hole. *Classical Quantum Gravity*, 22(6):1167–1190, Mar. 2005.
  - [17] F. de Felice. Repulsive phenomena and energy emission in the field of a naked singularity. *Astronomy and Astrophysics*, 34:15–19, 1974.
  - [18] F. de Felice. Classical instability of a naked singularity. *Nature*, 273:429–431, June 1978.
  - [19] V. Faraoni. Turnaround radius in modified gravity. *Physics of the Dark Universe*, 11:11–15, Mar. 2016.
  - [20] V. Faraoni, M. Lapiere-Léonard, and A. Prain. Turnaround radius in an accelerated universe with quasi-local mass. *Journal of Cosmology and Astroparticle Physics*, 2015(10):013–013, Oct. 2015.
  - [21] G. W. Gibbons and S. W. Hawking. Cosmological event horizons, thermodynamics, and particle creation. *Phys. Rev. D*, 15:2738–2751, May 1977.
  - [22] E. G. Gimon and P. Hořava. Over-Rotating Black Holes, Gödel Holography and the Hypertube, 2004.
  - [23] E. G. Gimon and P. Hořava. Astrophysical Violations of the Kerr Bound as a Possible Signature of String Theory. *Phys. Lett. B*, 672:299, 2009.
  - [24] Z. Gu and H. Cheng. The circular loop equation of a cosmic string in Kerr–de Sitter spacetimes. *Gen. Relativity Gravitation*, 39(1):1–7, Jan. 2007.
  - [25] E. Hackmann, B. Hartmann, C. Lämmerzahl, and P. Sirimachan. Test particle motion in the space-time of a Kerr black hole pierced by a cosmic string. *Phys. Rev. D*, 82(4):044024, Aug. 2010.
  - [26] K. Hioki and K.-i. Maeda. Measurement of the Kerr spin parameter by observation of a compact object’s shadow. *Phys. Rev. D*, 80(2):024042 (9 pages), July 2009.
  - [27] L. Iorio. Constraining the cosmological constant and the DGP gravity with the double pulsar PSR J0737-3039. *New Astronomy*, 14(2):196–199, Feb. 2009.
  - [28] V. Kagramanova, J. Kunz, and C. Lämmerzahl. Solar system effects in Schwarzschild–de Sitter space-time. *Phys. Lett. B*, 634(5–6):465–470, Mar. 2006.
  - [29] M. Kološ and Z. Stuchlík. Current-carrying string loops in black-hole spacetimes with a repulsive cosmological constant. *Phys. Rev. D*, 82(12):125012 (21 pages), Dec. 2010.
  - [30] F. Kottler. Über die physikalischen Grundlagen der Einsteinschen Gravitationstheorie. *Annalen der Physik*, 361(14):401–462, 1918.
  - [31] G. V. Kraniotis. Precise theory of orbits in general relativity, the cosmological constant and the perihelion precession of Mercury. pages 469–479.
  - [32] G. V. Kraniotis. Precise relativistic orbits in Kerr and Kerr–(anti-)de Sitter spacetimes. *Classical Quantum Gravity*, 21:4743–4769, 2004.
  - [33] G. V. Kraniotis. Periapsis and gravitomagnetic precessions of stellar orbits in Kerr and Kerr–de Sitter black hole spacetimes. *Classical Quantum Gravity*, 24:1775–1808, 2007.
  - [34] L. M. Krauss. The end of the age problem, and the case for a cosmological constant revisited. *Astrophys. J.*, 501(2):461–466, 1998.
  - [35] L. M. Krauss and M. S. Turner. The cosmological constant is back. *Gen. Relativity Gravitation*, 27(11):1137–1144, Nov. 1995.
  - [36] H. Kučáková, P. Slaný, and Stuchlík. Toroidal configurations of perfect fluid in the reissner-nordström-(anti-)de sitter spacetimes. *Journal of Cosmology and Astroparticle Physics*, 2011(01):033, 2011.
  - [37] K. Lake. Bending of light and the cosmological constant. *Phys. Rev. D*, 65(8, B):087301, Apr. 2002.
  - [38] A. D. Linde. *Particle Physics and Inflationary Cosmology*. Gordon and Breach, New York, 1990.
  - [39] A. Müller and B. Aschenbach. Non-monotonic orbital velocity profiles around rapidly rotating Kerr (anti-)de Sitter black holes. *Classical and Quantum Gravity*, 24:2637–2644, May 2007.
  - [40] T. Müller. Falling into a Schwarzschild black hole. *Gen. Relativity Gravitation*, pages 56–+, Feb. 2008.
  - [41] M. Olivares, J. Saavedra, C. Leiva, and J. R. Villanueva. Motion of charged particles on the Reissner–Nordström (anti-)de Sitter black hole spacetime. *Modern Phys. Lett. A*, 26(39):2923–2950, Dec. 2011.
  - [42] J. P. Ostriker and P. J. Steinhardt. The observational case for a low-density universe with a nonzero cosmological constant. *Nature*, 377(6550):600–602, Oct. 1995.
  - [43] D. Pérez, G. E. Romero, and S. E. Bergliaffa. Accretion discs around black holes in modified strong gravity. *Astronomy and Astrophysics*, 551:A4(15 pages), Mar. 2013.
  - [44] C. Pierre-Henri and T. Harko. Bose–Einstein Condensate general relativistic star. *Phys. Rev. D*, 86(6):064011, Sept. 2012.
  - [45] Planck Collaboration, P. A. R. Ade, N. Aghanim, C. Armitage-Caplan, M. Arnaud, M. Ashdown, F. Atrio-Barandela, J. Aumont, C. Baccigalupi, A. J. Banday, and et al. Planck 2013 results. XII. Diffuse component separation. *Astronomy and Astrophysics*, 571:A12, Nov. 2014.
  - [46] D. Pugliese and Z. Stuchlík. Ringed Accretion Disks: Equilibrium Configurations. *Astrophys. J. Suppl.*, 221(2):25, dec 2015.
  - [47] L. Rezzolla, O. Zanotti, and J. A. Font. Dynamics of thick discs around Schwarzschild–de Sitter black holes. *Astronomy and Astrophysics*, 412(3):603–613, Dec. 2003.
  - [48] A. G. Riess et al. Type Ia Supernova Discoveries at  $z > 1$  From the Hubble Space Telescope: Evidence for Past Deceleration and Constraints on Dark Energy Evolution. *Astrophys. J.*, 123:145, 2004.
  - [49] J. Schee, Z. Stuchlík, and M. Petrásek. Influence of the cosmic repulsion on the MOND model of the Magellanic Cloud motion in the field of Milky Way. *Journal of Cosmology and Astroparticle Physics*, 12:026, Dec. 2013.
  - [50] T. Schücker and N. Zaimen. Cosmological constant and time delay. *Astronomy and Astrophysics*, 484(1):103–106, June 2008.
  - [51] M. Sereno. On the influence of the cosmological constant

- on gravitational lensing in small systems. *Phys. Rev. D*, 77(4):043004, 2008.
- [52] Z. Sheng, C. Ju-Hua, and W. Yong-Jiu. Time-like geodesic structure of a spherically symmetric black hole in the brane-world. *Chinese Physics B*, 20(10):100401, 2011.
- [53] P. Slaný and Z. Stuchlík. Relativistic thick discs in the Kerr–de Sitter backgrounds. *Classical Quantum Gravity*, 22(17):3623–3651, 2005.
- [54] P. Slaný and Z. Stuchlík. Comment on ‘non-monotonic orbital velocity profiles around rapidly rotating kerr(anti-)de sitter black holes’. *Classical and Quantum Gravity*, 25(3):038001, 2008.
- [55] D. N. Spergel, R. Bean, O. Dore, M. R. Nolte, C. L. Bennett, J. Dunkley, G. Hinshaw, N. Jarosik, E. Komatsu, L. Page, H. V. Peiris, L. Verde, M. Halpern, R. S. Hill, A. Kogut, M. Limon, S. S. Meyer, N. Odegard, G. S. Tucker, J. L. Weiland, E. Wollack, and E. L. Wright. Three-year Wilkinson Microwave Anisotropy Probe (WMAP) observations: Implications for cosmology. *Astrophys. J. Suppl.*, 170(2):377–408, June 2007.
- [56] D. N. Spergel, R. Bean, O. Dore, M. R. Nolte, C. L. Bennett, J. Dunkley, G. Hinshaw, N. Jarosik, E. Komatsu, L. Page, H. V. Peiris, L. Verde, M. Halpern, R. S. Hill, A. Kogut, M. Limon, S. S. Meyer, N. Odegard, G. S. Tucker, J. L. Weiland, E. Wollack, and E. L. Wright. ThreeYear Wilkinson Microwave Anisotropy Probe ( WMAP ) Observations: Implications for Cosmology. *Astrophys. J. Suppl.*, 170(2):377–408, jun 2007.
- [57] Z. Stuchlík. Equatorial circular orbits and the motion of the shell of dust in the field of a rotating naked singularity. *Bull. Astronom. Inst. Czechoslovakia*, 31:129–144, 1980.
- [58] Z. Stuchlík. The radial motion of photons in Kerr metric. *Bulletin of the Astronomical Institutes of Czechoslovakia*, 32:40–52, 1981.
- [59] Z. Stuchlík. The motion of test particles in black-hole backgrounds with non-zero cosmological constant. *Bull. Astronom. Inst. Czechoslovakia*, 34(3):129–149, 1983.
- [60] Z. Stuchlík. An Einstein–Strauss–de Sitter model of the universe. *Bull. Astronom. Inst. Czechoslovakia*, 35(4):205–215, 1984.
- [61] Z. Stuchlík. Spherically symmetric static configurations of uniform density in spacetimes with a non-zero cosmological constant. *Acta Phys. Slovaca*, 50(2):219–228, Mar. 2000.
- [62] Z. Stuchlík. Influence of the Relict Cosmological Constant on Accretion Discs. *Modern Phys. Lett. A*, 20(8):561–575, Mar. 2005.
- [63] Z. Stuchlík, G. Bao, E. Østgaard, and S. Hledík. Kerr–Newman–de Sitter black holes with a restricted repulsive barrier of equatorial photon motion. *Phys. Rev. D*, 58(8):084003, Oct. 1998.
- [64] Z. Stuchlík and M. Calvani. Null geodesics in black-hole metrics with nonzero cosmological constant. *Gen. Relativity Gravitation*, 23(5):507–519, May 1991.
- [65] Z. Stuchlík and S. Hledík. Some properties of the Schwarzschild–de Sitter and Schwarzschild–anti-de Sitter spacetimes. *Phys. Rev. D*, 60(4):044006 (15 pages), Aug. 1999.
- [66] Z. Stuchlík and S. Hledík. Equatorial photon motion in the Kerr–Newman spacetimes with a non-zero cosmological constant. *Classical Quantum Gravity*, 17(21):4541–4576, Nov. 2000.
- [67] Z. Stuchlík and S. Hledík. Properties of the Reissner–Nordström spacetimes with a nonzero cosmological constant. *Acta Phys. Slovaca*, 52(5):363–407, Oct. 2002.
- [68] Z. Stuchlík, S. Hledík, and J. Novotný. General relativistic polytropes with a repulsive cosmological constant. *Phys. Rev. D*, 94:103513, Nov 2016.
- [69] Z. Stuchlík, S. Hledík, and K. Truparová. Evolution of Kerr superspinars due to accretion counterrotating thin discs. *Classical Quantum Gravity*, 28(15):155017, Aug. 2011.
- [70] Z. Stuchlík and M. Kološ. Acceleration of string loops in the Schwarzschild–de Sitter geometry. *Phys. Rev. D*, 85(6):065022 [13 pages], 2012.
- [71] Z. Stuchlík and M. Kološ. String loops in the field of braneworld spherically symmetric black holes and naked singularities. *Journal of Cosmology and Astroparticle Physics*, 2012:008, 2012.
- [72] Z. Stuchlík and J. Kovář. Pseudo-Newtonian gravitational potential for Schwarzschild–de Sitter spacetimes. *INTJMD*, 17(11):2089–2105, 2008.
- [73] Z. Stuchlík and J. Schee. Appearance of Keplerian discs orbiting Kerr superspinars. *Classical Quantum Gravity*, 27(21):215017 (39 pages), Nov. 2010.
- [74] Z. Stuchlík and J. Schee. Influence of the cosmological constant on the motion of Magellanic Clouds in the gravitational field of Milky Way. *Journal of Cosmology and Astroparticle Physics*, 9:018–018, Sept. 2011.
- [75] Z. Stuchlík and J. Schee. Comparison of general relativistic and pseudo-Newtonian description of Magellanic-clouds motion in the field of Milky Way. *Internat. J. Modern Phys. D*, 21(4):1250031, Apr. 2012.
- [76] Z. Stuchlík and J. Schee. Observational phenomena related to primordial Kerr superspinars. *Classical and Quantum Gravity*, 29(6):065002, 2012.
- [77] Z. Stuchlík and J. Schee. Ultra-high-energy collisions in the superspinning Kerr geometry. *Classical Quantum Gravity*, 30(7):075012, Apr. 2013.
- [78] Z. Stuchlík and P. Slaný. Equatorial circular orbits in the Kerr–de Sitter spacetimes. *Phys. Rev. D*, 69:064001, 2004.
- [79] Z. Stuchlík, P. Slaný, and S. Hledík. Equilibrium configurations of perfect fluid orbiting Schwarzschild–de Sitter black holes. *Astronomy and Astrophysics*, 363(2):425–439, Nov. 2000.
- [80] Z. Stuchlík, P. Slaný, and J. Kovář. Pseudo-Newtonian and general relativistic barotropic tori in Schwarzschild–de Sitter spacetimes. *Classical Quantum Gravity*, 26(21):215013 (34 pp), Nov. 2009.
- [81] Z. Stuchlík, P. Slaný, G. Török, and M. A. Abramowicz. Aschenbach effect: Unexpected topology changes in the motion of particles and fluids orbiting rapidly rotating Kerr black holes. *Phys. Rev. D*, 71(2):024037, Jan. 2005.
- [82] J. R. Villanueva, J. Saavedra, M. Olivares, and N. Cruz. Photons motion in charged Anti-de Sitter black holes. *Astrophys. and Space Sci.*, 344(2):437–446, Dec. 2012.
- [83] L. Wang, R. R. Caldwell, J. P. Ostriker, and P. J. Steinhardt. Cosmic concordance and quintessence. *Astrophys. J.*, 530(1):17–35, 2000.
- [84] L. Wang and H. Cheng. The evolution of circular loops of a cosmic string with periodic tension. *Phys. Lett. B*, 713(1):59–62, 2012.